for clusters where the range of the potential could be similarly varied to cause range-induced transitions in cluster structure. However, it remains an intriguing possibility.

tures we have found at the appropriate ρ_0 to be very similar to the actual structures of these clusters. Interestingly, the results lead us to predict that neutral clusters of C_{60} molecules exhibit decahedral and fcc structures at small sizes because of the short range of the intermolecular potential. This basic conclusion has been confirmed in studies using more realistic potentials[95,118]. However, this prediction for neutral cluster differs from experimental results[58] for charged clusters for which icosahedral structures are observed up to 55 molecules for $(C_{60})_N^+$ and 147 molecules for $(C_{60})_N^{++}$. Given the exceptionally large polarizability of C_{60}, though, it is not unreasonable that the introduction of a long range Coulomic term would significantly affect the energetic competition between morphologies. Therefore, it would be very interesting if this dramatic difference in structure between charged and neutral clusters could be observed experimentally, say by electron diffraction.

In contrast, making predictions for metal clusters from our results is much more difficult because the range of the potential is only one factor influencing structure. In particular, many-body terms may also be important[62,63]. These terms may affect the relative surface energies of {111} and {100} faces, and so alter the energetic competition between icosahedral, decahedral and fcc structures[102]. For example, in a study of lead clusters cuboctahedra are always found to be lower in energy than icosahedra because the surface energies of {111} and {100} faces are nearly equal[104]. The value of our results is in providing candidate structures for comparison with the increasingly detailed structural information being provided by experiments, such as chemical probe studies[66–68], and for theoretical studies with more realistic, but also more computationally expensive, descriptions of the interactions.

Our results also allow us to comment on a global optimization method proposed by Stillinger and Stillinger in which the PES is deformed by increasing the range[92]. We have to echo Chang and Berry's caution[119] that although increasing the range of a potential does lead to a simplification of the PES it can also cause large changes in the relative stability of different minima. The global minimum when a potential is long-ranged may be very different from the global minimum at the conditions of interest.

For mixtures of spherical colloidal particles and non-adsorbing polymer, the range of the attractive interaction between the colloidal particles can be systematically varied by changing the size of the polymer[120]. This effect has been used to study experimentally the phase diagram for such colloidal systems as a function of the range of the interaction[121–123]. We know of no physically realizable system

example the cause is clearly the differences in the energy spectrum of minima for the two morphologies. In general, then, the global minimum provides a reasonable guide to the finite temperature structural properties of a cluster, which can be usefully supplemented by a knowledge of other low energy minima on the PES.

If there is a unique low energy global minimum separated by a large energy gap from higher energy structures it is appropriate to associate the solid-like structure of the cluster with this single minimum. This would be the case, for example, for the icosahedron 55B at intermediate ranges of the potential. For the LJ potential, microcanonical simulations have shown that the 55-atom cluster resides only in the icosahedral potential well up to an energy of 40ϵ (measured with respect to the bottom of the icosahedral well) above which the formation of surface defects is observed and then complete melting[108–112]. However, when there is a set of low energy minima with very similar energies, at all but very low temperatures an equilibrium ensemble of clusters will contain a mixture of these isomers. It is therefore more appropriate to associate the 'structure' with this set of minima rather than the global minimum alone. For example, this would be the case for 55C, which has three other low energy isomers with the same n_{nn}.

In the above discussion we have been considering the equilibrium structural properties. However, we also need to consider the question of kinetic versus thermodynamic products. How important are the low potential energy structures in practice? When will they actually be found in an experiment? Van de Waal has suggested that kinetic factors could be essential in the growth of fcc rare-gas clusters and the nucleation of fcc solid from the LJ liquid[113,114]. Indeed an extremely good fit is obtained to electron diffraction results for argon clusters from non-optimal structures that involve cross-twinning to allow rapid growth[115,116]. As we noted earlier, the effect of increasing the size and decreasing the range of the potential is to increase the complexity of the PES. Therefore, as the range of the potential decreases the formation of glassy or amorphous clusters, rather than the lowest energy structure, becomes more likely. Whether this is the case for the larger clusters we have studied when the potential is short-ranged would require further investigation. The results for bulk C_{60} may also provide some insight into this question. When formed by vapour phase deposition C_{60} gives an amorphous soot[117], and only forms the crystalline phase on recrystallization from benzene.

In this chapter we have been considering the effect of the range of attraction of pair interactions on cluster structure. As rare gas clusters and clusters of C_{60} molecules can be reasonably modelled by pair potentials we would expect the struc-

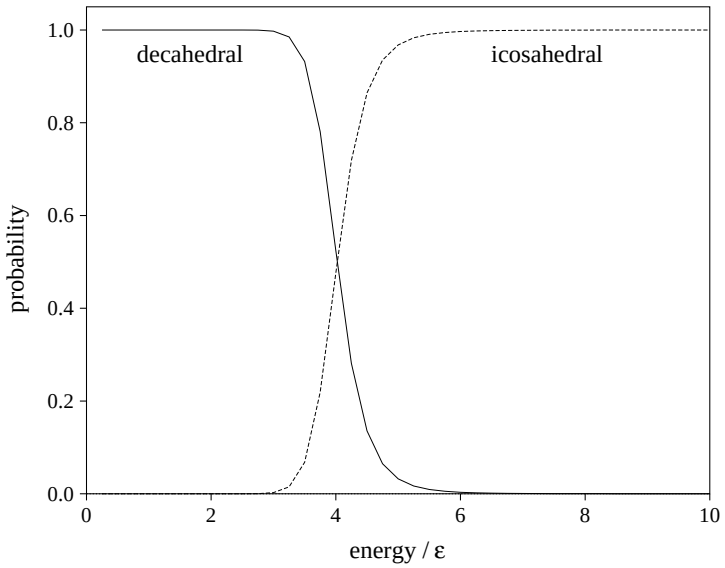

FIGURE 2.19: Calculated equilibrium values for the microcanonical probability that an M_{75} cluster at $\rho_0 = 6$ has an icosahedral or a decahedral structure as a function of the total energy. The energy is measured with respect to the bottom of the well of the Marks' decahedron, 75C.

seen that the equilibrium structure changes from decahedral to icosahedral when the total energy is only $4\,\epsilon$ above the bottom of the lowest well, which corresponds to a reduced temperature of $0.018\,\epsilon\,k^{-1}$. It is likely that such a transition would not be observed until higher energies because of the free energy barrier involved. In fact we once observed this transition in an MD run started from structure 75C. The run was 1×10^6 time steps long and at a total energy of 74ϵ above the lowest well.

This calculation also helps to explain why 75C has not been previously reported as the lowest energy structure for the much-studied LJ potential. Global optimization algorithms are often based upon tracking the free energy global minimum as the temperature is decreased. This is the principle behind the widely-used simulated annealing method[107]. However, such methods will not find the global minimum if a change in the free energy global minimum occurs at a temperature where the rate of isomerization is so low that a transition to the new structure cannot occur on the time scale of the simulation.

We should not conclude from the above calculation, though, that the global minimum is not important in understanding cluster structures. This example is probably an exception rather than the rule. Such a transition is only likely to occur for values of ρ_0 near to where the global minimum changes and in the above

TABLE 2.3: The ten lowest energy decahedral and icosahedral minima found for M_{75} at $\rho_0 = 6$.

decahedral			icosahedral		
Energy/ϵ	Point Group	n_{nn}	Energy/ϵ	Point Group	n_{nn}
-351.472365	D_{5h}	319	-351.177041	C_1	328
-349.500086	C_1	317	-351.139799	C_1	328
-349.498552	C_1	317	-351.135122	C_s	328
-349.498393	C_1	317	-350.984741	C_1	328
-349.496058	C_1	317	-350.912649	C_1	328
-349.489864	C_1	317	-350.890122	C_1	328
-349.275647	C_1	317	-350.874153	C_1	328
-348.606586	C_1	316	-350.686821	C_1	327
-348.332763	C_1	316	-350.612539	C_s	329
-347.636104	C_1	315	-350.464407	C_1	327

PES. The thermodynamic properties of a collection of minima can be approximated by superposition of the density of states from each minimum, as described in detail in Chapter 3.

Here we apply this method to M_{75} at $\rho_0 = 6$ to illustrate the limitations of finite temperature structural predictions based on knowledge of the global minimum alone. Sets of low energy decahedral and icosahedral minima were obtained by performing minimizations from configurations generated by low energy MD runs starting from icosahedral and decahedral regions of configuration space. The ten lowest energy minima of each sample are given in Table 2.3. For M_{75}, the Marks' decahedron, 75C, is the most stable cluster at $\rho_0 = 6$. There is an energy gap of 2ϵ to the next lowest energy decahedral isomer (Table 2.3). At this value of ρ_0 the lowest energy icosahedral structure is only 0.3ϵ higher in energy than 75C and there are many icosahedral isomers of similar energy (Table 2.3). In fact we found 31 icosahedral isomers which were of lower energy than the second lowest energy decahedral isomer. From this it might be expected that as the energy is increased the density of states of the icosahedral isomers would become larger than the decahedral isomers, and so the structure would change from decahedral to icosahedral with increasing energy or temperature.

We calculated within the harmonic approximation the equilibrium probabilities that the structure would be icosahedral or decahedral as a function of the micro-canonical total energy. The results are given in Figure 2.19. From this it can be

disordered array of disclinations in another part of the cluster.

Other interesting structures are also seen. 47A, 50A and 59A seem to have a mixture of Mackay and anti-Mackay overlayers present. 64A is formed from the rhombic tricontahedron 45A by the extension of the structure along a three-fold axis and the addition of a ring of atoms in the centre of the cluster. However, for the larger clusters it becomes harder to recognize any motifs in the structures, and some just seem to be disordered tangles of disclinations. Disordered polytetrahedral structures involving a network of disclination lines will be considered further when the structure of liquids is discussed in detail in §4.4. It suffices to note here that the nearest-neighbour peak in the radial distribution function of these structures is broader than for the ordered structures considered in the preceding sections, and that, furthermore, these clusters when reoptimized to larger values of ρ_0 correlate with structures that are in the lower energy range of the band of minima associated with the liquid-like state of clusters. It is interesting that theoretical studies of sodium clusters have shown that amorphous structures are lower in energy than regular structures up to at least 340 atoms, the largest size considered in that study[106]. The present results allow us to identify the cause of these disordered structures as the relatively long range of the sodium potential.

Since most minima in this structural class do not have a common lattice, or packing scheme, it is difficult to predict the low energy structures, and so most have been found by one of the global optimization methods mentioned in §2.2.2. Fortunately, these methods are most likely to succeed at long range because the PES is smoother and has fewer minima than at shorter ranges. Another consequence of the lack of lattice structure is that the differentiation between nearest neighbours and next-nearest neighbours becomes ambiguous and the decomposition of equation 2.2 more arbitrary. For these clusters, we choose to define n_{nn} using a cutoff at ρ_0=4 which corresponds to the distance at which the pair energy is $0.6\,\epsilon$.

2.4 Discussion

In this chapter we have attempted to find the global minimum for Morse clusters as a function of ρ_0 and the number of atoms. The global minimum represents the equilibrium structure at zero Kelvin. However, we need to consider how important the global minimum is in determining the structure at finite temperature. To answer this question we have to examine the effects of other local minima on the

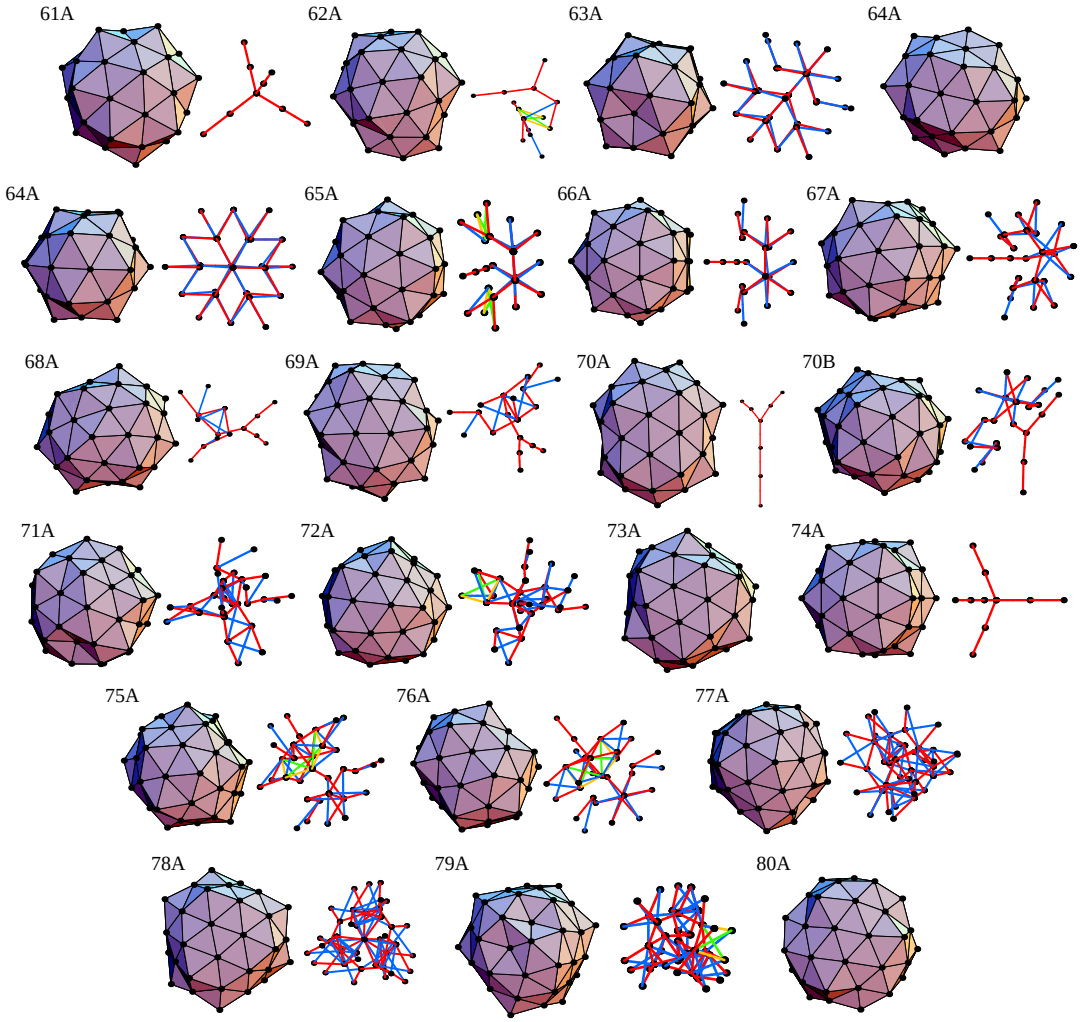

FIGURE 2.18: continued.

ima (Figure 2.18). The one exception is structure 38A, which is similar to the icosahedral structures 38B and 38C, but has two positive disclinations running through the structure in a strange double helical twist.

The most stable disclinated polytetrahedral structures occur at N=53, 57, and 61 (Figure 2.6). These are the sizes for which 'anti-Mackay' overlayers of 15A, 16A and the 17-atom structure involving a tetrahedral arrangement of disclinations are completed. In these structures, those interior atoms not lying on a disclination line are icosahedrally coordinated. Many other minima are related to these stable structures: 51A and 52A are based on 53A but with missing vertex atoms; similarly, 59B and 60A are based on 61A; and 70A and 74A are based on 57A and 61A, respectively, but with an additional 13-atom cap which extends one of the 'arms' of the disclination network. Furthermore, many of the other structures include parts of the disclination networks of 53A, 57A and 61A, but combined with a more

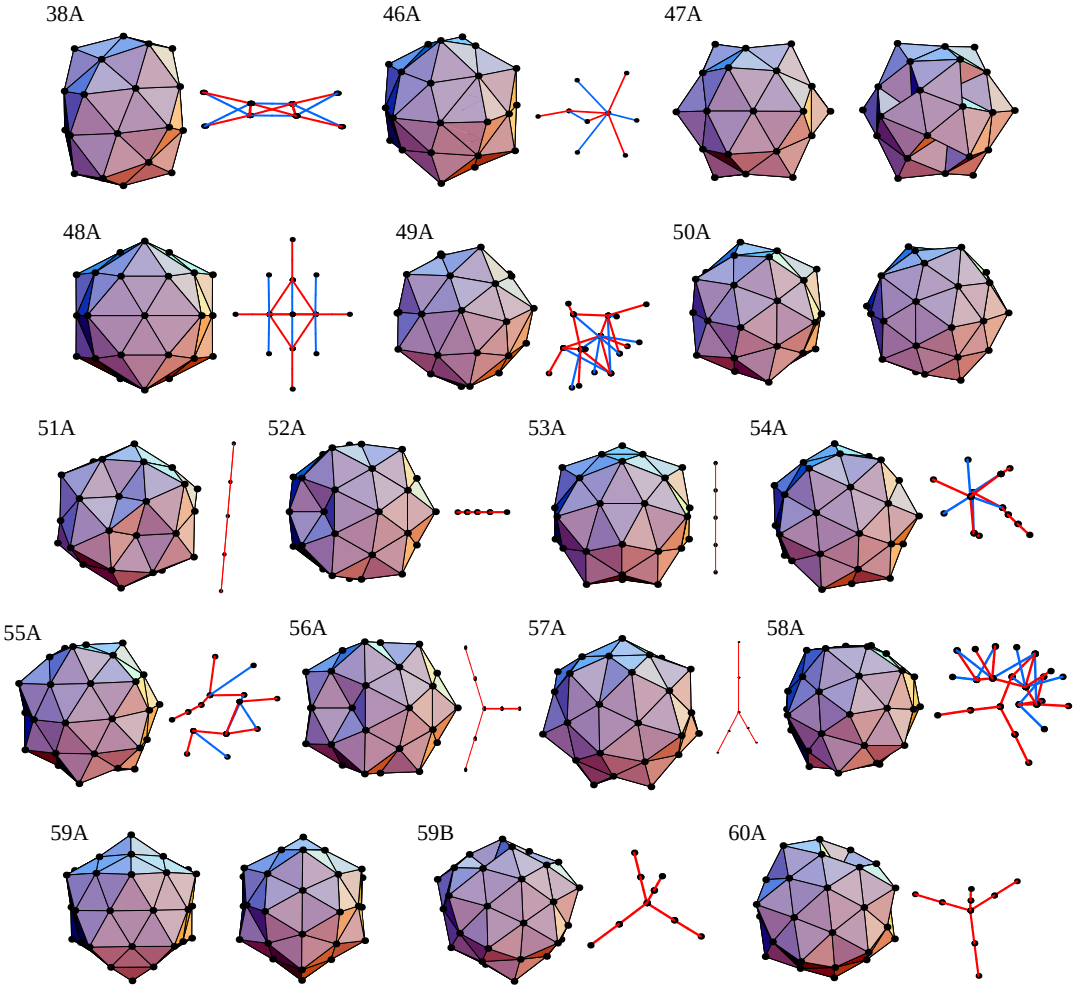

FIGURE 2.18: Global minima at low values of ρ_0 for $N \geq 38$. If appropriate, the disclination network is displayed next to each structure. $-72°$ disclinations are represented by red lines, and $+72°$ disclinations by blue lines. $-144°$ disclinations by green lines, and $+144°$ disclinations by yellow lines.

strains, and for M_{18}, say, would only have the same n_{nn} as the icosahedral 18B.

The structures 11A, 12A, 14A, 15A and 16A are all deltahedral, and so growth can occur on these structures in 'anti-Mackay' or 'Mackay' sites (Figure 2.9), in the same way as for the icosahedron 13A. However, if one considers the addition of a hexagonal pyramidal cap to the most stable of the Kasper polyhedra, 15A, the result is a D_{6h} structure with a positive disclination running the length of the symmetry axis (a disclinated equivalent of the double icosahedron 19A) that has only the same n_{nn} as the icosahedral structure 22A. Disclinated polytetrahedral structures cannot compete with the disclination-free polytetrahedral structures produced by the anti-Mackay overlayer to the icosahedron. Only once this growth sequence is completed at N=45 are structures with disclinations again global min-

assigned to the Voronoi polyhedron of the atom to which it is closest. This allows nearest neighbours to be defined as those atoms whose Voronoi polyhedra share a face. The Delaunay network that results from joining all such nearest neighbours is the dual of the Voronoi construction and divides all space into tetrahedra. This definition of a nearest neighbour has been termed geometric, rather than physical (e.g. using a cutoff distance), and the division of space into tetrahedra that this method achieves is artificial in the sense that it is independent of whether a polytetrahedral description is appropriate. In practice we determined the Voronoi polyhedra by using the fact that a set of four atoms constitutes a Delaunay tetrahedron if the sphere that touches all four atoms contains no other atoms[105]. The centre of this sphere is then a vertex of the Voronoi polyhedron of each atom. As the number of tetrahedra around a nearest-neighbour bond is the same as the number of sides on the face common to the Voronoi polyhedra of both nearest neighbours, disclination lines can then be assigned. However, problems can occur in assigning the Delaunay network if there are more than four atoms exactly on the surface of the sphere. Such a degeneracy, which only occurs as a result of symmetry, renders the analysis non-unique. This is the case for the 55-atom Mackay icosahedra and for bulk close-packed solids because of the presence of octahedra, but is not a problem here since we only apply the method to clusters that are polytetrahedral in character. One further consideration is that the analysis should not be applied to nearest-neighbour bonds between the surface atoms of a cluster.

The smallest global minimum that involves a disclination line is 11A. It involves a central atom surrounded by a 10-atom coordination shell, which has the structure of the hollow cluster 10A. The encapsulation of the central atom gives the structure a larger n_{nn} than the incomplete icosahedron 11B, but results in a larger strain energy (Table 2.2); the surface is in tension. The structure involves a single positive disclination line running through the centre of the cluster. Similarly, for N=12 and 14-16 structures with a single coordination shell become lower in energy than structures based on the icosahedron at long range. For those with $N > 13$ the surface is in compression. As we shall see in §4.4, structures 11A, 12A, 14A, 15A and 16A correspond to Kasper polyhedra. Of these structures 15A is the most stable as measured by the range of ρ_0 for which it is the global minimum. For 17A, the surface has the same structure as 16A, but there are two atoms in the centre of the cluster. The second lowest energy structure of M_{17} at $\rho_0 = 3$ has a 16-coordinate central atom, which is the node for a tetrahedral array of disclinations. Structures with a more highly coordinated central atom involve increasingly large

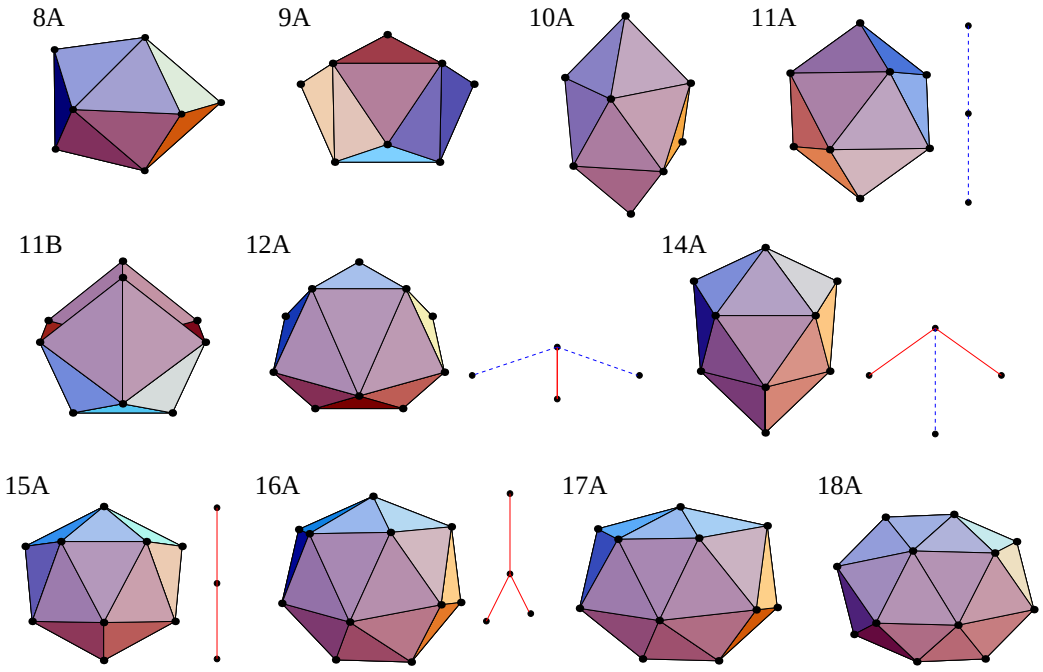

FIGURE 2.17: Global minima for small clusters at low values of ρ_0. If appropriate, the disclination network is displayed next to each structure. $-72°$ disclinations are represented by red lines, and $+72°$ disclinations by blue lines.

defects called disclination lines running along the bond. Those bonds with more than five tetrahedra are termed negative disclinations (if there are six it is a $-72°$ disclination, if there are seven a $-144°$ disclination, ...) and those with fewer than five tetrahedra are positive disclinations (if there are four it is a $+72°$ disclination and if there are three a $+144°$ disclination). Most of the structures associated with low ρ_0 are polytetrahedral structures that involve disclinations. Although packing five tetrahedra around a nearest-neighbour bond involves some strain, the strain energy associated with packing more or less tetrahedra around a bond is greater. Therefore, structures involving disclinations are only likely to be lowest in energy for long-ranged potentials for which the associated strain can be most easily accommodated, and only if the structures have a larger n_{nn} than disclination-free structures. A $-72°$ disclination line involves less strain than a $+72°$ disclination line as can be deduced from the gap that remains when five regular tetrahedra share a common edge (Figure 2.3a). Consequently, structures which involve only negative disclinations, or an excess of them, are more common amongst the low ρ_0 global minima.

To calculate the network of disclination lines in a structure, one must first partition space according to the Voronoi procedure, in which each point in space is

atom truncated tetrahedron with the faces covered by four seven-atom hexagonal overlayers occupying hcp sites with respect to the underlying tetrahedron. The smaller of those structures based on 59D have no overlayer on one face of the underlying tetrahedron. The stability of 59D comes from the combination of its high proportion of {111} faces and spherical shape. Interestingly, if atoms are added to one of the grooves in the structure a decahedral-like axis results, suggesting a possible transformation route between decahedral and closed-packed clusters.

It is worth noting that the cuboctahedron is not the lowest energy close-packed structure for N=55. In fact, it has five fewer nearest neighbours than structure 55D. Consequently, one has interpret with caution those studies in which cuboctahedra have been compared with Mackay icosahedra[75,102–104]; the cuboctahedra are likely to be suboptimal fcc structures, thus making the comparison unfair.

2.3.4 Structures at long range

In this subsection, we consider those structures which become the global minimum only at low values of ρ_0. We have restricted our study to those clusters with $\rho_0 \geq 3$, since we know of no cluster system for which longer-ranged potentials are of relevance. It may well be that further changes in the global minima occur[60] at lower ρ_0. The low ρ_0 structures that we have found separate into two size ranges, those with N close to N=13 and those with $N > 45$; they are shown in Figures 2.17 and 2.18, respectively.

The group of structures associated with low ρ_0 are close to spherical in shape and in the main are highly strained in order to maximize n_{nn}. The exceptions are 8A, 9A and 10A (Figure 2.17). These clusters have smaller values of n_{nn} than the other low energy minima (Figure 2.8), but are more stable because of a larger contribution from E_{nnn}; the next-nearest neighbour shell is significantly closer than for the incomplete icosahedra. In each case the structures are roughly spherical but do not have an atom in the centre of the cluster.

The majority of the other structures are polytetrahedral, that is the whole volume of the cluster can be divided into tetrahedra with atoms at the vertices. As we noted in §2.3.1, the 13-atom icosahedron is polytetrahedral. In this structure, each nearest-neighbour bond between the centre and a vertex is the common edge of five tetrahedra. This is also true of all the nearest-neighbour bonds of the rhombic tricontahedron (45A) which do not lie on the surface. Nearest-neighbour bonds which are surrounded by a different number of tetrahedra are said to have

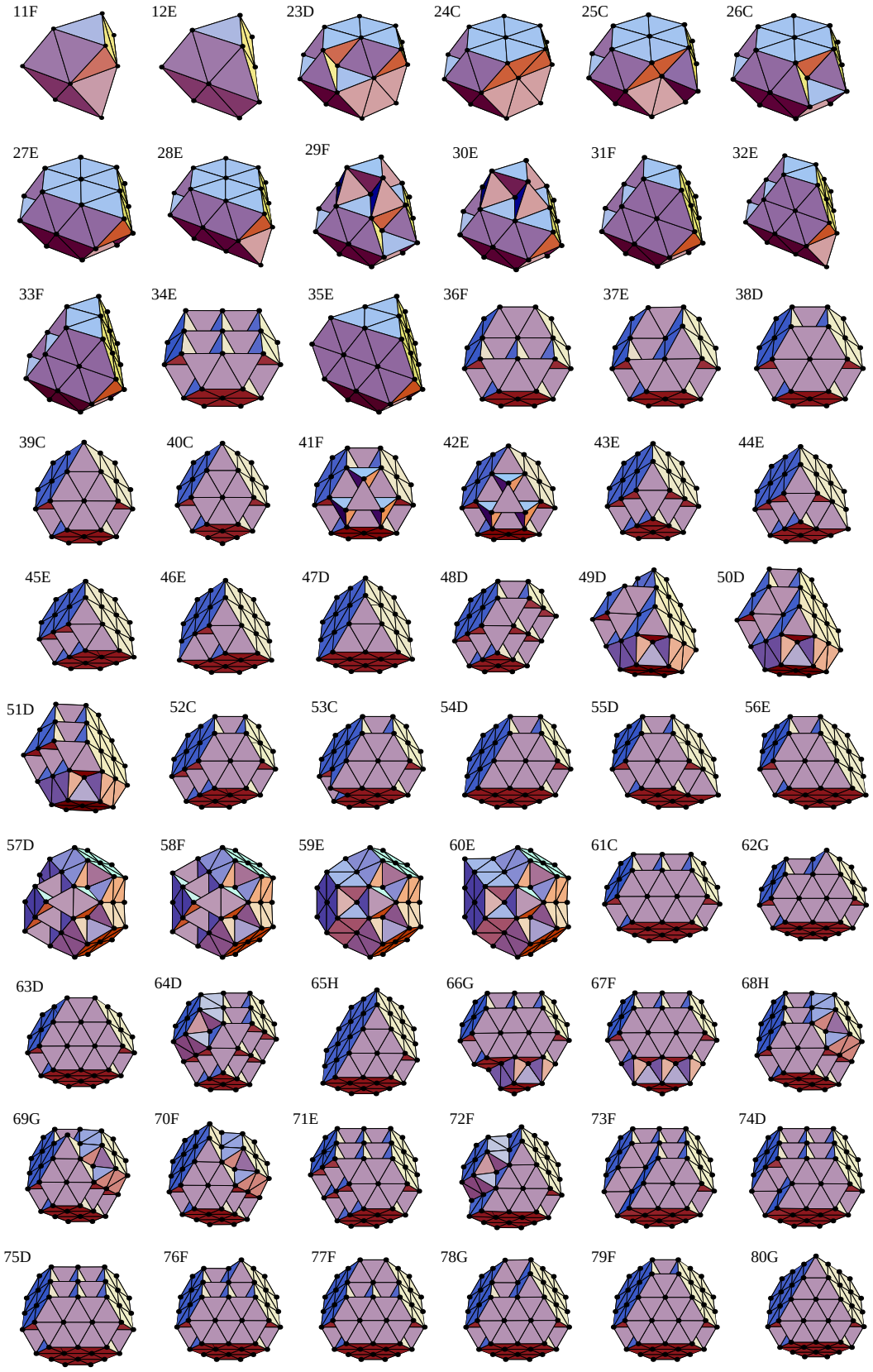

FIGURE 2.16: Global minima based on close-packing.

2.3.3 Close-packed clusters

The close-packed global minima are illustrated in Figure 2.16. They have a diverse range of structures: there are 30 minima that are pure fcc, 10 that are pure hcp and 20 that involve a mixture of stacking sequences and twin planes. The global minima are broadly based on four structures: the hcp 26C, the two truncated octahedra, 38D and 79F; and the tetrahedral 59D,

The 38-atom truncated octahedron is the most stable fcc cluster in the size range we consider. It becomes the global minimum at the lowest value of ρ_0 (4.76) of any of the close-packed structures. Curiously, there are two ranges of ρ_0 for which it is the global minimum. At long range, E_{nnn} represents a significant part of the total energy. The truncated octahedron is most stable for $4.76 < \rho_0 < 5.40$ because it is approximately spherical and so has a larger value of E_{nnn} than the more oblate icosahedral structure 38E. For shorter-ranged potentials, the contribution of E_{nnn} diminishes and so 38E becomes the global minimum for $5.40 < \rho_0 < 6.95$ because it has a larger n_{nn}. Then for $\rho_0 > 6.95$ the truncated octahedron again becomes the global minimum because it has a lower strain energy than 38E. There is a growing body of experimental evidence for the importance of truncated octahedra. EXAFS (extended x-ray absorption fine structure) spectra of small gold clusters suggest that truncated octahedral clusters are present, particularly the 38-atom truncated octahedron[101]. Gold clusters passivated by alkylthiolate molecules selectively form truncated octahedra, which can even be isolated and formed into superlattices[7]. The structure is also observed for ligated 38-atom platinum clusters[5].

Most of the structures with between 38 and 79 atoms are broadly based on a growth sequence that goes between the two truncated octahedra. It proceeds by addition of overlayers to four of the $\{111\}$ faces and by capping any new (2×2) $\{100\}$ faces created. For example, there is a peak in $\Delta_2 E$ at $\rho_0 = 14$ that is caused by the low energy of 52C; this structure is formed by the addition of complete overlayers to two faces of 38D. For a number of sizes, the structures that result from adding the overlayers in fcc or hcp sites with respect to $\{111\}$ faces have the same n_{nn}. For these cases the structures with the hcp overlayers are often lower in energy because they have a larger value of E_{nnn}—some of the third nearest neighbours are at 1.63 rather than 1.73 times the equilibrium pair separation. Examples include 41F, 42C, 64D, 66G, 67F, 68H, 69G, 70F and 72F.

The exceptions to the above growth sequence are those structures—49D, 50D, 51D, 57D, 58F and 60E—that are based on structure 59D. This structure is a 31-

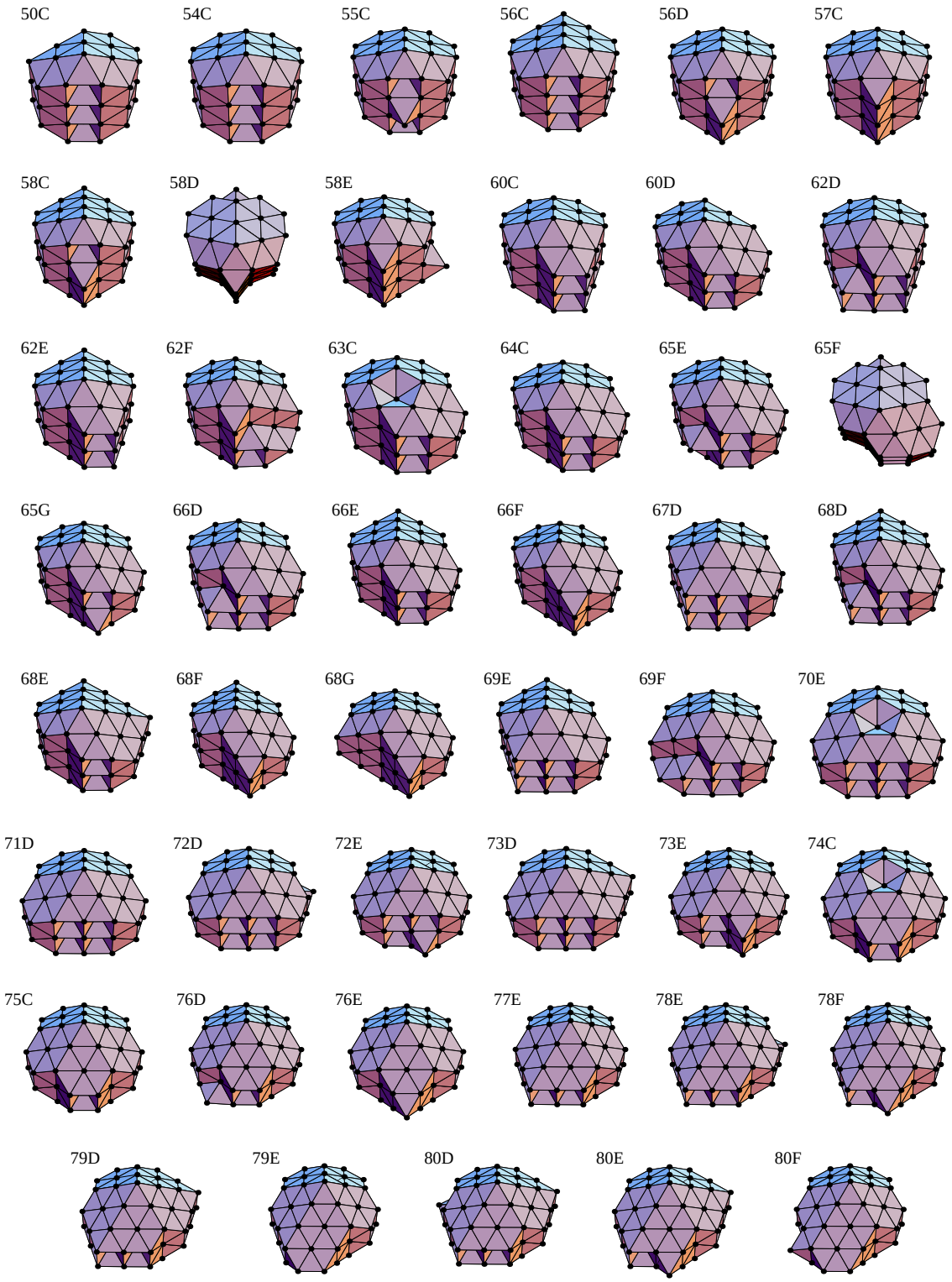

FIGURE 2.15: Global minima based upon a decahedron with five atoms along the fivefold axis.

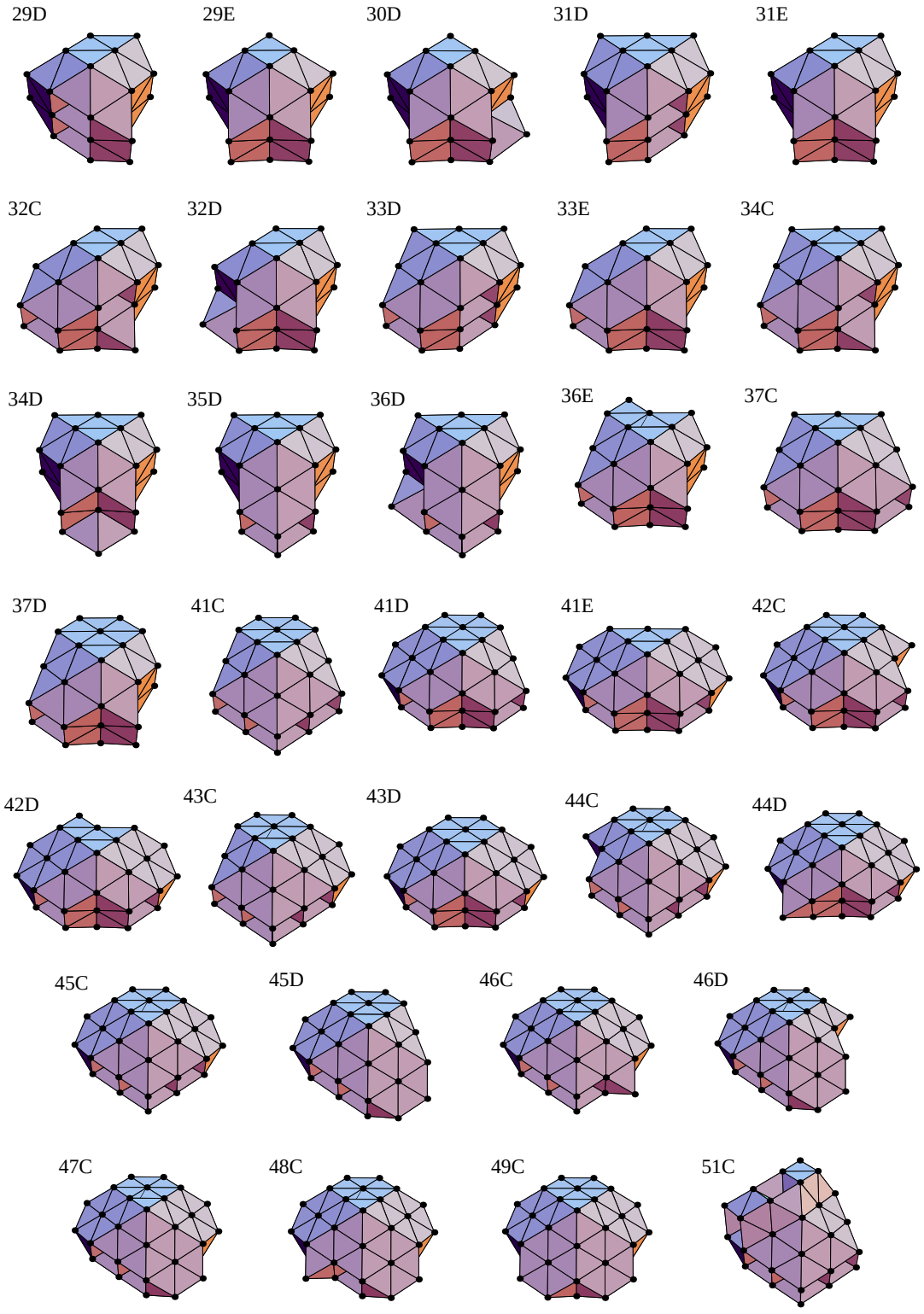

FIGURE 2.14: Global minima based upon a decahedron with four atoms along the fivefold axis.

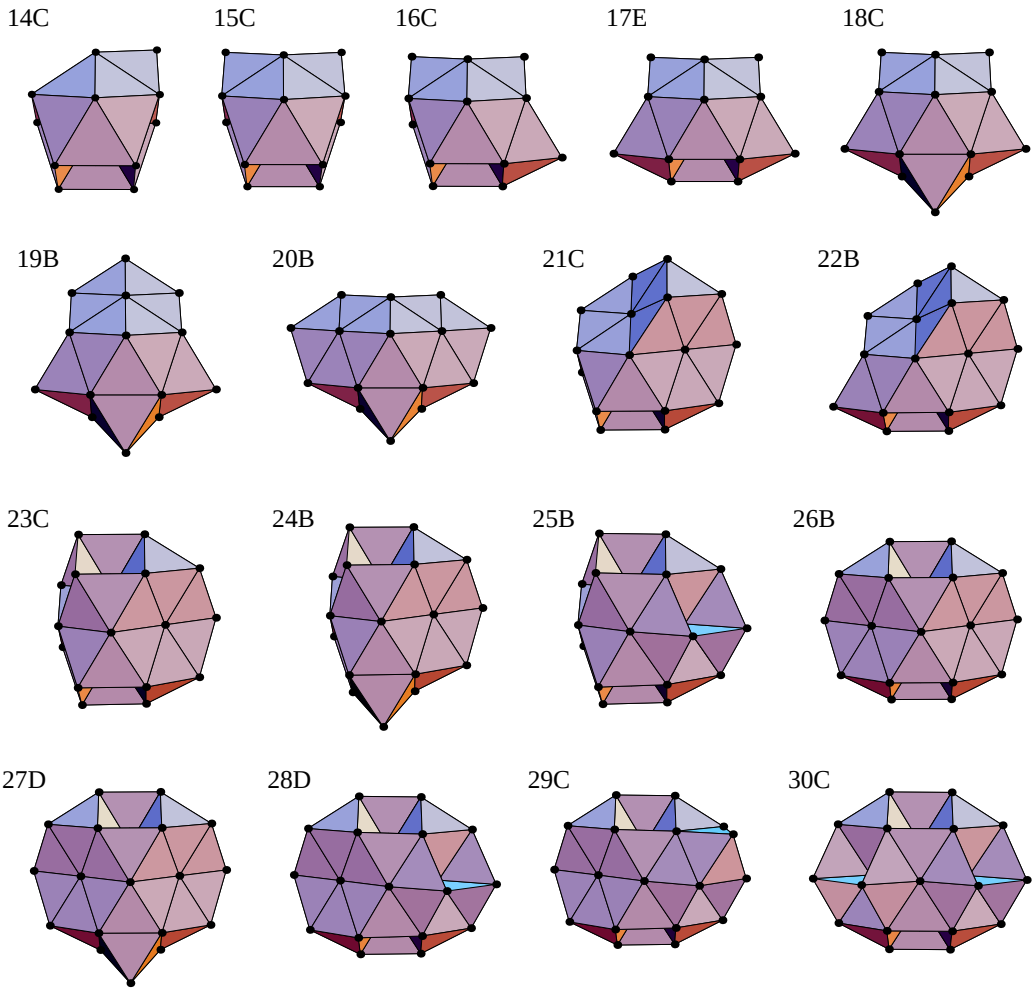

FIGURE 2.13: Global minima based upon a decahedron with three atoms along the fivefold axis.

surrounding the fivefold axis in the hcp sites with respect to the five fcc tetrahedra that make up the decahedral structures. These structures are more favourable even though they are more strained than the usual decahedral structures, because they have a larger n_{nn}. For N=21–30 these structures are actually fragments of the 55-atom Mackay icosahedron. The difference from the icosahedral structures is that the growth occurs from the five tetrahedra at the bottom of the Mackay icosahedron, rather than the centre.

As we mentioned in §2.2.1 the complete Marks' decahehedron, 75C, is particularly stable. The value of ρ_0 at which it becomes the global minimum (5.81) is the lowest of any of the decahedral structures. It is also the global minimum[71] for LJ_{75}. This stability is also indicated by the large peak in $\Delta_2 E$ for ρ_0=10 and 14. Other particular stable structures occur at N=64 and 71; these are fragments of 75C with 3 and 4 {100} faces of the Marks' decahedron complete.

The first structure in this size range with a Mackay overlayer is 78D. It is expected that the size at which the crossover from an anti-Mackay to a Mackay overlayer again increases with the range of the potential, but to confirm this prediction the study would need to be extended to larger sizes. There are also three icosahedral global minimum, 69B, 70C and 71B, which do not fit neatly into either the Mackay or anti-Mackay category. The surface layer has a Mackay-like character, but it is not in correct alignment with the underlying icosahedron. The overlayer has been given a twist about one of the fivefold axis in order to collapse some of the half octahedra at the edge of the overlayer into trigonal bipyramids in a multiple diamond-square-diamond (DSD) process[100]. In fact for M_{71} at ρ_0=5, the lowest energy Mackay structure is a transition state which mediates a multiple DSD rearrangement between two permutational isomers of 71B.

Figure 2.7 provides an illuminating illustration of the variation of the icosahedral energies with size. The complete Mackay icosahedra represent narrow minima, which are separated by broad maxima corresponding to structures with an incomplete outer shell. At ρ_0=6 it is only near the top of these maxima that fcc and decahedral structures begin to have similar energies, such as at N=38 and 75.

2.3.2 Decahedral clusters

The decahedral global minima are shown in Figures 2.13–2.15. The structures have been grouped by the number of the atoms along the fivefold axis of the pentagonal bipyramid upon which they are based.

The growth sequence for the decahedral clusters is quite simple; they grow by capping exposed {100} faces and by filling in the grooves produced by the re-entrant {111} faces. As this process progresses the structure changes from prolate to approximately spherical to oblate. This cycle begins again when a prolate cluster with a longer decahedral axis becomes lower in energy than the oblate cluster (e.g. at $N \approx 30$ and 50). For the clusters based upon a pentagonal bipyramid with 5 atoms along the fivefold axis ($N \geq 50$), the growth proceeds asymmetrically—the decahedral axis does not always pass through the center of the cluster. For example, for 54C the surface structure of the 75-atom Marks' decahedron is completed on one side of the cluster before atoms are added to the other.

Deviations from this basic growth scheme occur for N=21–30 (Figure 2.13) and 51C. These structures are formed by addition of atoms to the {111} faces

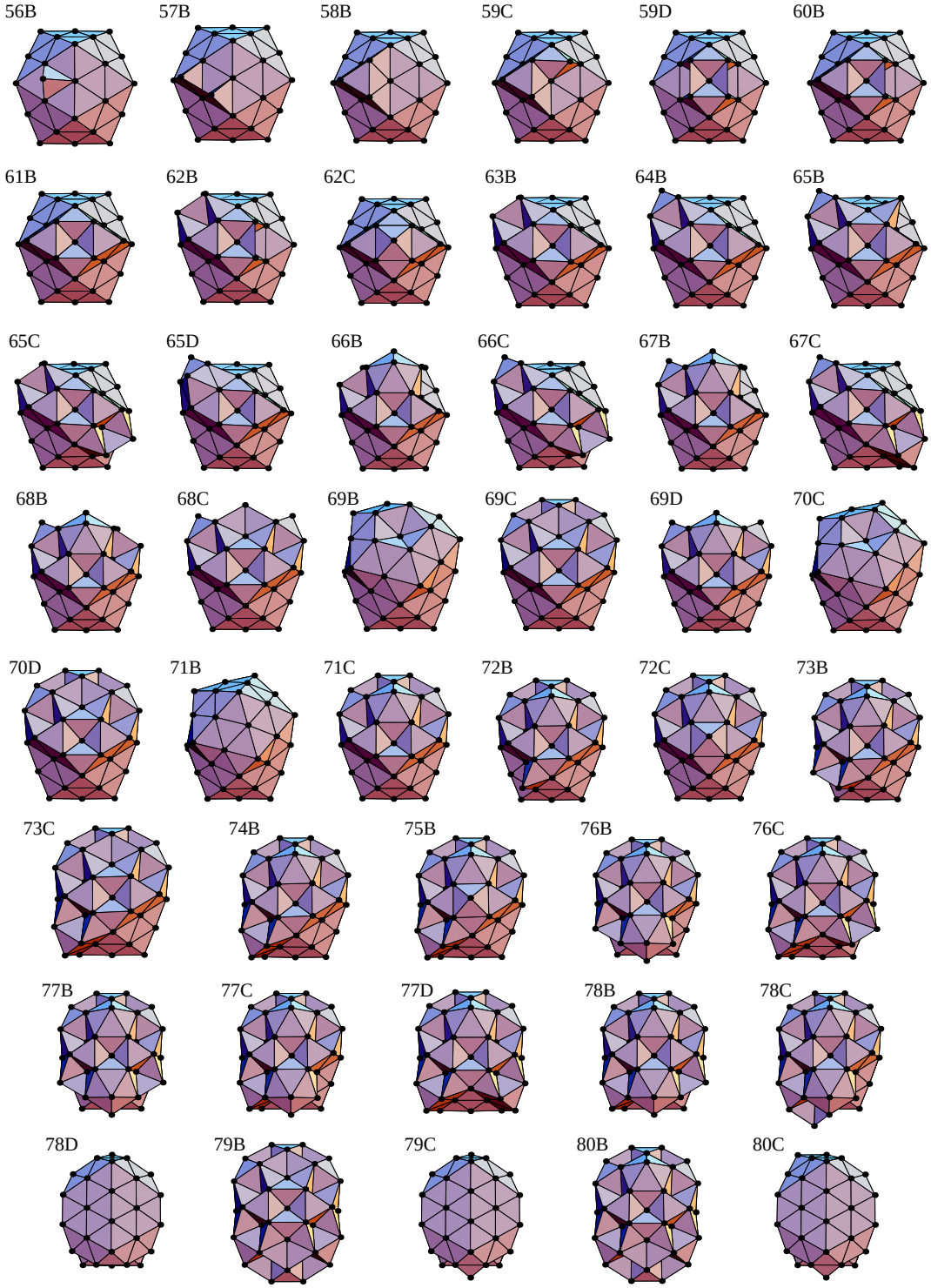

FIGURE 2.12: Icosahedral global minima formed by growth from the 55-atom Mackay icosahedron.

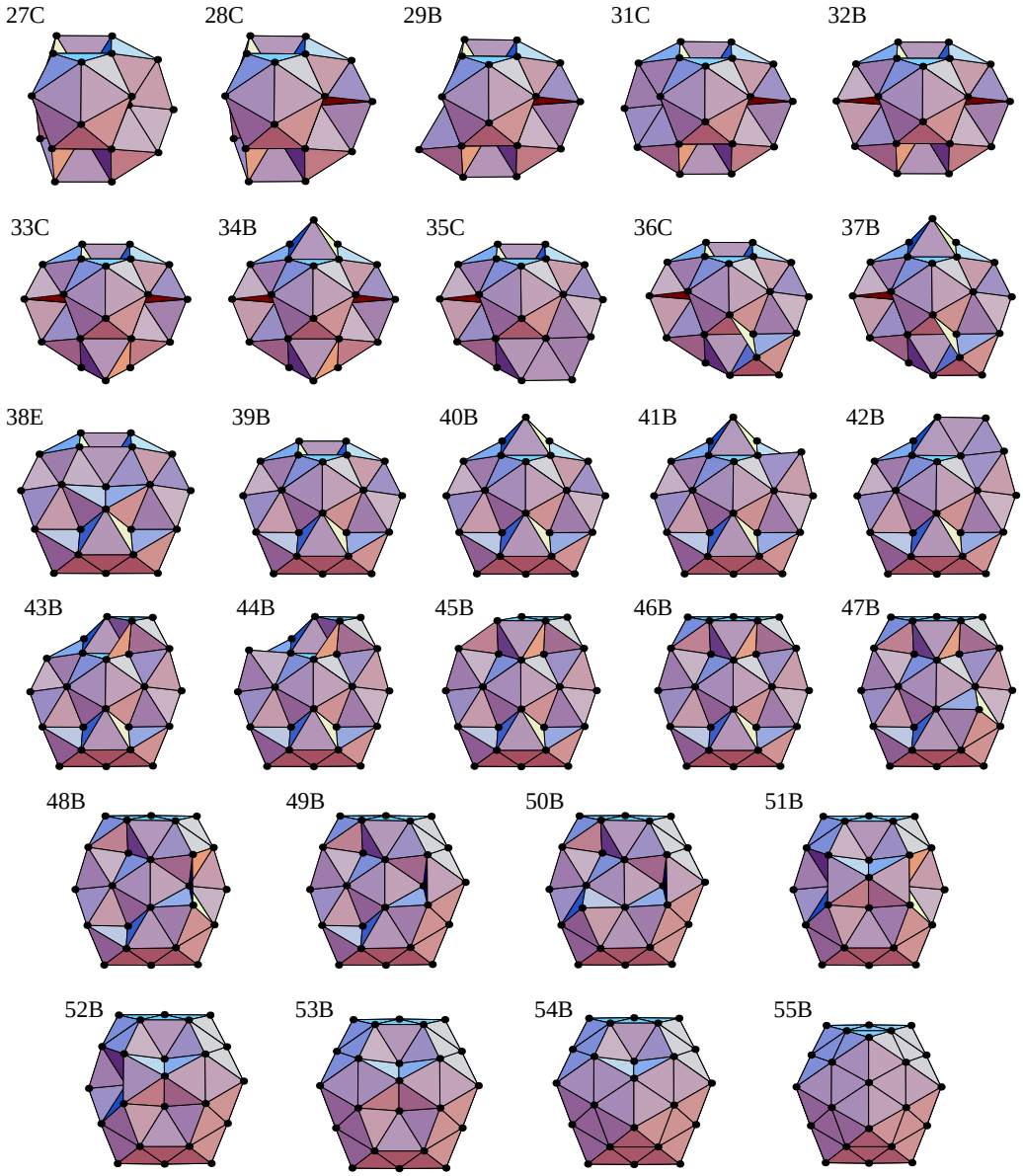

FIGURE 2.11: Icosahedral global minima formed by growth of an Mackay overlayer on the 13-atom icosahedron.

octahedra that are visible in the surface layers of the anti-Mackay clusters. The most prominent peak in $\Delta_2 E$ due to an anti-Mackay structure occurs at N=71 for ρ_0=6. This corresponds to an overlayer which completely covers the five faces surrounding a vertex of the underlying icosahedron. There are smaller peaks at N=58, 61, and 64, which correspond to complete coverage of one, two and three faces, respectively.

Similar to 38E, structure 69C has a vertex atom missing from the underlying Mackay icosahedra. There are also structures (62C, 65D, 72C and 75B) where an atom is added to the surface of the overlayer rather than to the Mackay icosahedra.

At $\rho_0 = 6$ the Mackay overlayer is occupied for $N \geq 32$. This compares to $N \geq 31$ for LJ clusters; as expected the results are very similar. In *ab initio* molecular dynamics calculations for lithium clusters[97], the anti-Mackay overlayer is lowest in energy up to $N = 45$. Similarly, polytetrahedral structures were observed in a tight-binding study of sodium clusters up to the largest size considered N=34 (for which 34A was the most stable structure)[98]. These effects are nicely explained by the long range of alkali metal potentials.

Especially stable structures with an anti-Mackay overlayer occur when the icosahedral coordination of a vertex atom is complete. These structures give rise to the peaks in $\Delta_2 E$ at N=19, 23 26, 29, 34 and 45 for ρ_0=3; only the first four of these peaks are seen at ρ_0=6, and only the first at ρ_0=10 (Figure 2.6). Some of these magic numbers have been observed in mass spectroscopic studies of rare gases[47,48] and even barium[99]. The centres of the icosahedra in these structure form a dimer for 19A, an equilateral triangle for 23A, a tetrahedron for 26A, a trigonal bipyramid for 29A, a pentagonal bipyramid for 34A, and an icosahedron for 45A. At a number of sizes there is more than one global minimum with an anti-Mackay overlayer. The transitions between these structures are related to slight differences in the value of E_{strain}. Also illustrated in Figure 2.10 is structure 23B, which is made up of two face-sharing icosahedra. It can be formed from structure 17B by the addition of six atoms not to the icosahedron but to the atoms which are part of the overlayer.

The first global minimum with a Mackay overlayer occurs at N=27. Especially stable structures occur at those sizes for which complete faces of the 55-atom Mackay icosahedra are missing. These structures give rise to the peaks at N=39, 46 and 49 for ρ_0=6 and correspond to 5, 2 and 1 missing faces, respectively. Again, these magic numbers have been seen in mass spectra of rare gases[48].

Structure 38E has an atom missing from a vertex of the original 13-atom icosahedron to allow the overlayer to complete a particularly stable form. This structure was not found in Northby's study of icosahedral LJ clusters, even though it is the lowest energy LJ icosahedral cluster[73].

The icosahedral global minima with more than 55 atoms are shown in Figure 2.12. As for the 13-atom icosahedron, growth initially occurs at the anti-Mackay sites, because this results in structures with larger n_{nn}. Completion of this overlayer occurs for a cluster with 127 atoms. The vertex atoms of the 55-atom Mackay icosahedron become icosahedrally coordinated, but the edge atoms have a decahedral (13B) coordination shell (this is clearly visible for 59C) leading to the half

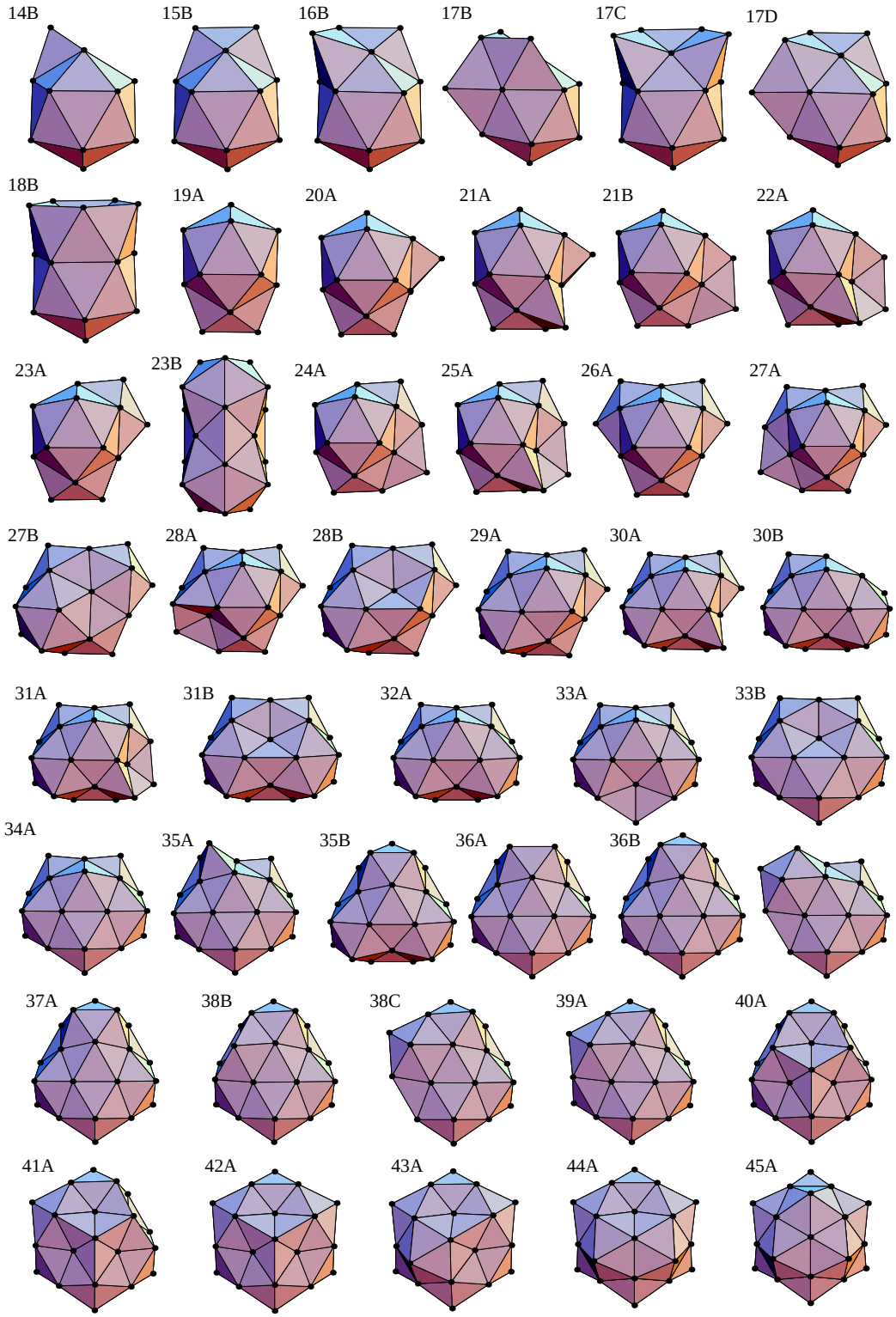

FIGURE 2.10: Icosahedral global minima formed by growth of an anti-Mackay overlayer on the 13-atom icosahedron, except structure 23B which is composed of two face-sharing icosahedra.

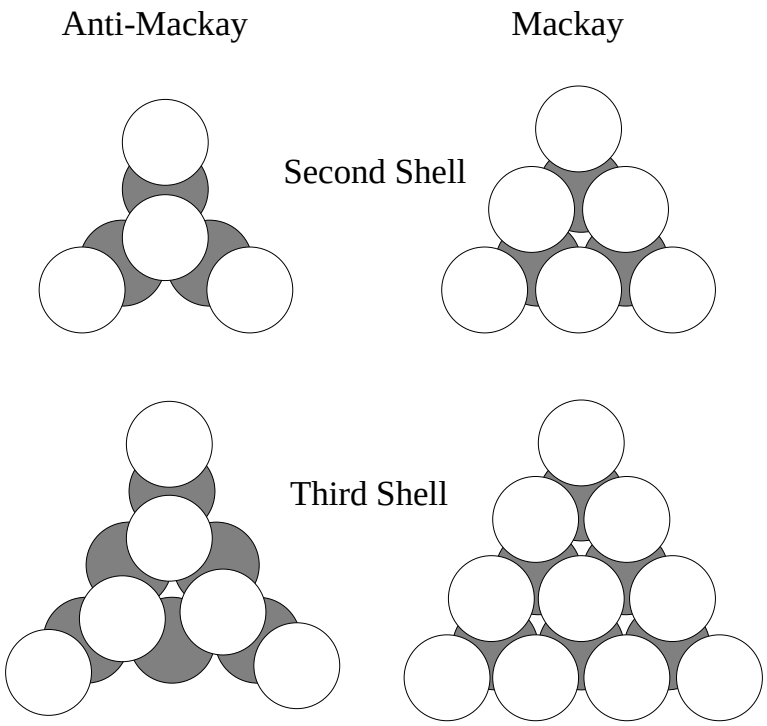

FIGURE 2.9: Atomic positions for the two possible overlayers of the icosahedron, anti-Mackay (left) and Mackay (right). These are shown for a single face of the icosahedron.

made famous by C_{60}; indeed, it is even a particularly stable shell for the coverage of a C_{60} molecule by alkaline earth metal atoms[96]. In previous studies, the anti-Mackay overlayer has been referred to as the polyicosahedral[43–45] or the face-capping overlayer[50]. Such names are reasonable for growth on the 13-atom icosahedron, but are confusing for growth on larger Mackay icosahedra.

The icosahedral structures with an anti-Mackay overlayer are illustrated in Figure 2.10 and those with an Mackay overlayer in Figure 2.11. Growth from the 13-atom icosahedron begins in the anti-Mackay positions, because these do not include any low-coordinate edge sites, thus giving the structures a larger n_{nn}. However, at some critical size the Mackay overlayer becomes lower in energy, because of the larger strain energies associated with the anti-Mackay overlayer. Further growth then leads to the next Mackay icosahedron. The size at which this change occurs depends on the range of the potential; it is given by the dashed line of negative slope that divides the icosahedral region of the phase diagram (Figure 2.5). The crossover size increases with the range of the potential; a long-ranged potential can accommodate the greater strain associated with the anti-Mackay overlayer more easily.

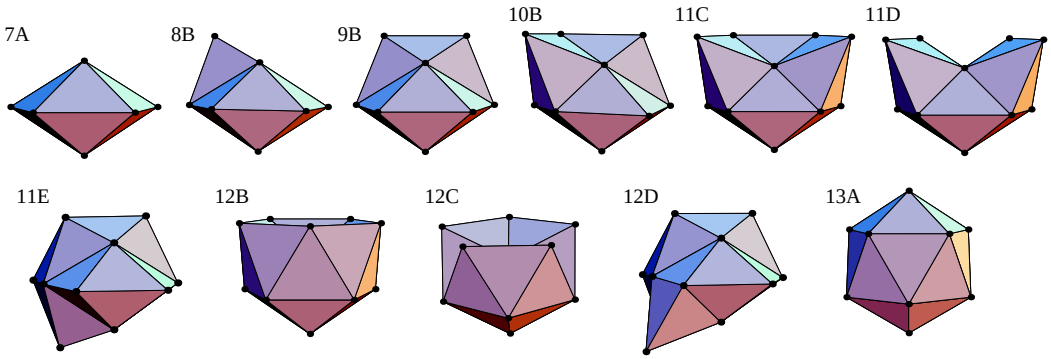

FIGURE 2.8: Global minima for $N \leq 13$ which are formed by growth on the 7-atom pentagonal bipyramid and which lead to the 13-atom icosahedron.

2.3.1 Icosahedral clusters

The growth sequence that leads from the 7-atom pentagonal bipyramid to the 13-atom icosahedron is shown in Figure 2.8. The growth occurs by the capping of the faces on one half of the bipyramid. For M_{11} and M_{12}, related structures become the global minimum at short range. Firstly, a symmetry breaking of structures 11C and 12B occurs. This results in the loss of one (11D) or two (12C) nearest-neighbour bonds, but also allows the other nearest-neighbour contacts to relax closer to the pair equilibrium distance. At still larger ρ_0, structures 11E and 12D, which involve capping of the faces on both sides of the pentagonal bipyramid, become lowest in energy. These structures have fewer nearest neighbours, but they are also less strained. All the structures shown in Figure 2.8 are polytetrahedral, in the sense that the whole of the cluster can be divided into tetrahedra with atoms at the vertices.

Addition of atoms to the 13-atom icosahedron can occur in two ways. The two types of overlayer that result are illustrated in Figure 2.9. One growth mode continues the fcc packing of the twenty strained tetrahedra making up the icosahedron, and leads to the 55-atom Mackay icosahedron (Figure 2.1b). This growth mode introduces octahedral interstices, and so the resulting structures are no longer polytetrahedral. The other growth mode involves sites which are hcp with respect to the tetrahedra, and has been termed the anti-Mackay overlayer. For growth on the 13-atom icosahedron, this overlayer preserves polytetrahedral character. Each of the vertices of the original icosahedron becomes icosahedrally coordinated, and the structure that results from the completion of this overlayer, 45A, is a rhombic tricontahedron; it is an icosahedron of interpenetrating icosahedra. Interestingly, the rhombic tricontahedron is the face-dual of the truncated icosahedron

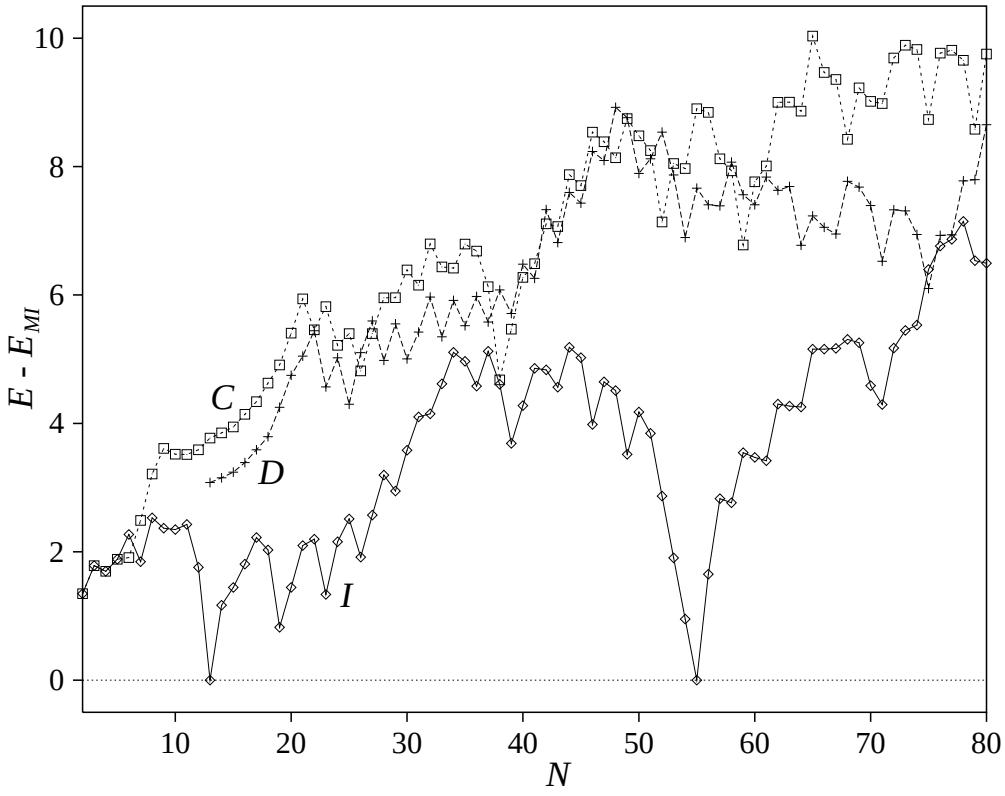

FIGURE 2.7: Comparison of the energies of icosahedral (solid line with diamonds), decahedral (dashed line with crosses) and close-packed (dotted line with squares) M_N clusters at ρ_0=6. The energy zero is E_{MI}, the interpolated energy of Mackay icosahedra. $E_{MI} = -3.0354 + 0.2624N^{1/3} + 8.8400N^{2/3} - 6.8381N$ and was obtained by fitting to the first four Mackay icosahedra (N=13, 55, 147 and 309).

for LJ clusters with peaks due to especially stable icosahedral clusters. At higher values of ρ_0 peaks corresponding to especially stable close-packed and decahedral clusters begin to occur. The plot at ρ_0=14 is very similar to that recently obtained for C_{60} clusters using the Girifalco potential[95]. Similarly, if the energy is normalized by subtracting a suitable function of N, again particularly stable sizes stand out (Figure 2.7).

In the following subsections we will look at the growth sequences for each structural class in more detail. As well as the three ordered morphologies, we also examine the unusual structures that occur for the larger clusters at low ρ_0, which, as we will see, involve a mixture of order and disorder.

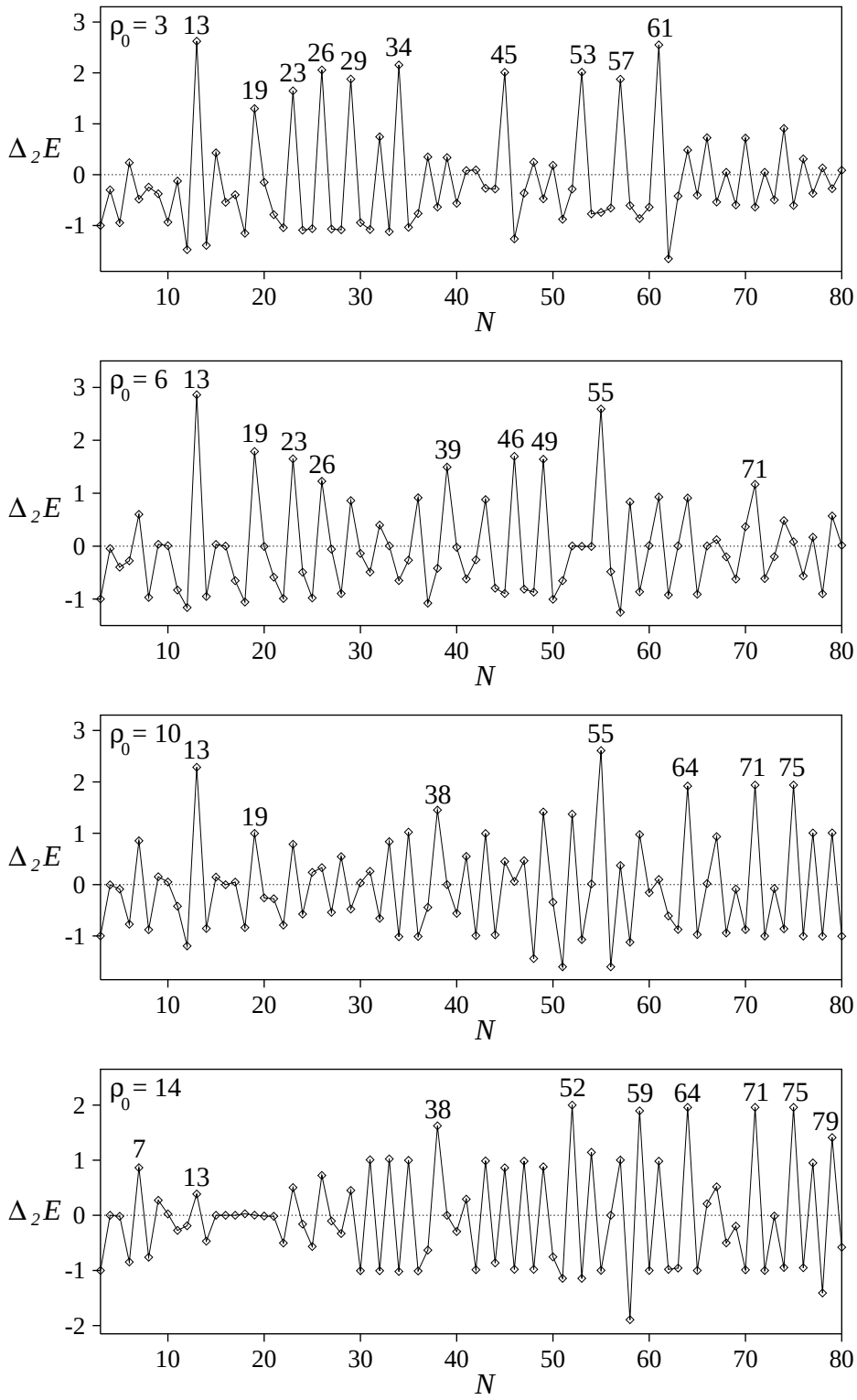

FIGURE 2.6: Plots of $\Delta_2 E$ as a function of N for ρ_0=3, 6, 10 and 14 as marked.

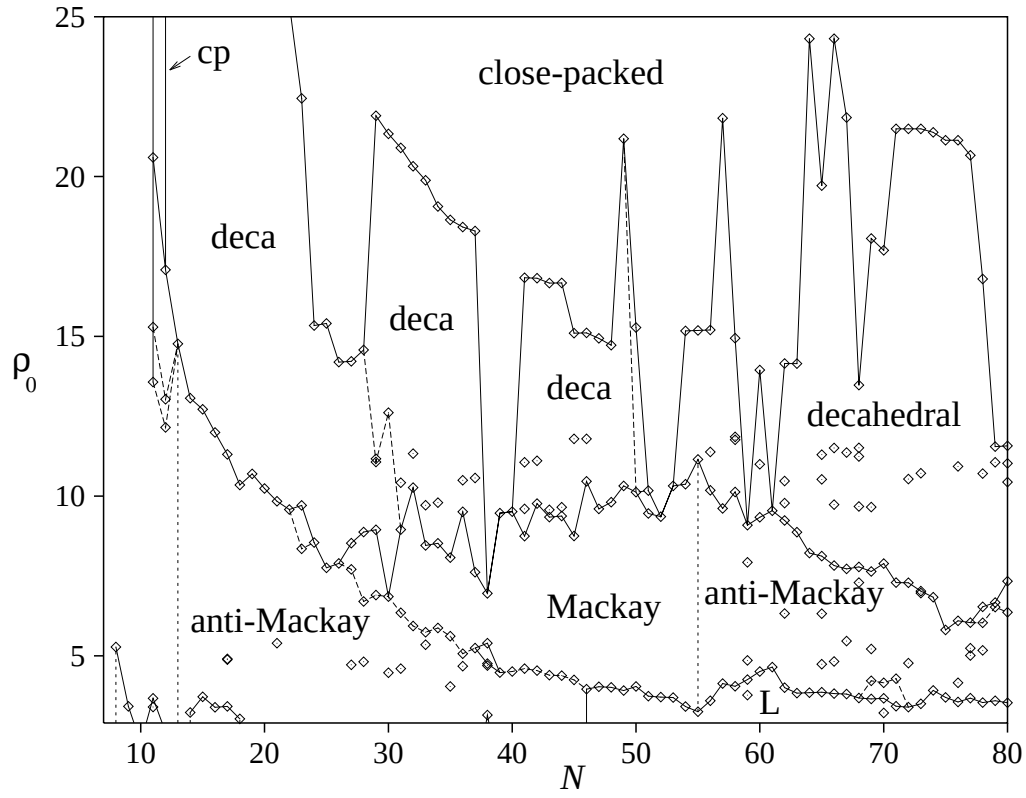

FIGURE 2.5: Zero temperature 'phase diagram' showing the variation of the lowest energy structure with N and ρ_0. The data points are the values of ρ_0 at which the global minimum changes. The lines joining the data points divide the phase diagram into regions where the global minima have similar structures. The solid lines denote the boundaries between the four main structural types—icosahedral, decahedral, close-packed and those associated with low ρ_0 (L)—and the dashed lines internal boundaries within a structural type, e.g. between icosahedral structures with Mackay and anti-Mackay overlayers, or between decahedral structures with different length decahedral axes.

sensitive, because the range of ρ_0 for which the decahedral structure is most stable changes dramatically even when the difference in n_{nn} between the decahedral and close-packed structures changes by one.

Sizes for which a morphology is the lowest in energy for a particularly large range of ρ_0 indicate that the structure is especially stable. The optimal structures shown in Figure 2.1 are particularly good examples of this. Another indicator of sizes of especial stability is provided by $\Delta_2 E(N) = E(N+1) + E(N-1) - 2E(N)$. Peaks in $\Delta_2 E$ have been found to correlate well with the magic numbers (sizes at which clusters are particularly abundant) observed in mass spectroscopic studies of clusters formed in molecular beams[94]. Plots of $\Delta_2 E$ are shown in Figure 2.6 for a number of values of ρ_0. Unsurprisingly, the plot for ρ_0=6 is very similar to that

TABLE 2.2: continued.

	PG	n_{nn}	E_{strain}	$\rho_0 = 3$	$\rho_0 = 6$	$\rho_0 = 10$	$\rho_0 = 14$	ρ_{min}	ρ_{max}
74A	C_{3v}	357		**-622.680**					3.92
74B	C_s	324	18.513	-614.020	**-346.611**	-308.886		3.92	6.83
74C	C_{5v}	313	0.699	-610.492	-345.200	**-316.651**	**-312.441**	6.83	21.38
74D	C_s	310	0.035		-342.317	-314.324	-310.745	21.38	
75A	C_s	364		**-633.513**					3.70
75B	C_1	328	18.559	-630.521	-351.177	-312.987	-296.599	3.70	5.81
75C	D_{5h}	319	0.718		**-351.472**	**-322.644**	**-318.407**	5.81	21.14
75D	C_{4v}	316	0.035		-348.841	-320.398	-316.758	21.14	
76A	C_s	370		**-644.952**					3.56
76B	C_1	334	21.847	-642.129	-355.971	-315.525	-298.049	3.56	4.16
76C	C_1	333	19.297	-641.559	**-356.250**	-317.225	-300.489	4.16	6.10
76D	C_s	323	0.737		-356.085	**-326.697**	-322.387	6.10	10.93
76E	C_{2v}	323	0.718		-355.772	-326.683	**-322.414**	10.93	21.14
76F	C_s	320	0.035		-353.246	-324.440	-320.764	21.14	
77A	C_1	368		**-656.080**	-349.696				3.68
77B	C_s	339	22.562	-650.116	-361.293	-319.898		3.68	5.01
77C	C_1	339	22.076		-361.416	-320.372	-302.897	5.01	5.24
77D	C_s	338	19.503	-647.494	**-361.591**	-322.075		5.24	6.04
77E	C_{2v}	328	0.749		-361.521	**-331.754**	**-327.372**	6.04	20.66
77F	C_s	325	0.035		-358.645	-329.483	-325.771	20.66	
78A	C_3	384		**-667.576**					3.54
78B	C_1	344	22.724	-664.006	-366.727	-324.815	-307.287	3.54	5.18
78C	C_1	344	22.651		**-366.761**	-324.883	-307.076	5.18	6.04
78D	C_s	338	11.849		-366.723	-330.163	-315.401	6.04	6.53
78E	C_1	332	0.769		-366.132	**-335.807**	-331.349	6.53	10.71
78F	C_s	332	0.749	-650.436	-365.872	-335.796	**-331.379**	10.71	16.80
78G	C_s	330	0.036		-364.252	-334.558	-330.784	16.80	
79A	C_1	385		**-678.940**	-358.580				3.59
79B	C_{2v}	348	19.381	-673.565	**-372.832**	-332.365		3.59	6.53
79C	C_{2v}	343	11.973		-372.466	-335.139	-320.223	6.53	6.67
79D	C_{2v}	337	0.783	-663.444	-371.568	**-340.862**	-336.332	6.67	11.06
79E	C_s	337	0.752	-659.186	-371.199	-340.834	-336.380	11.06	11.55
79F	O_h	336	0.036		-370.784	-340.632	**-336.796**	11.55	
80A	C_3	387		**-690.578**					3.53
80B	C_s	354	21.858	-683.221	**-378.333**	-335.898		3.53	6.36
80C	C_1	348	12.120		-377.972	-340.072	-324.944	6.36	7.34
80D	C_1	341	0.806	-674.292	-376.176	**-344.911**	-340.304	7.34	10.44
80E	C_s	341	0.783		-375.919	-344.904	-340.340	10.44	11.02
80F	C_s	341	0.752	-668.582	-375.572	-344.878	-340.387	11.02	11.57
80G	C_{4v}	340	0.036		-375.075	-344.669	**-340.803**	11.57	

TABLE 2.2: continued.

	PG	n_{nn}	E_{strain}	$\rho_0 = 3$	$\rho_0 = 6$	$\rho_0 = 10$	$\rho_0 = 14$	ρ_{min}	ρ_{max}
67A	C_s	318		**-544.754**	-297.548				3.80
67B	C_s	289	15.345	-539.667	-308.980	-276.565		3.80	5.46
67C	C_2	288	12.945	-538.179	**-309.130**	-278.090	-263.853	5.46	7.72
67D	C_{2v}	279	0.677		-307.349	**-282.172**	-278.396	7.72	11.36
67E	C_{2v}	279	0.674		-307.234	-282.166	**-278.401**	11.36	21.85
67F	C_{3v}	276	0.032		-304.942	-279.933	-276.681	21.85	
68A	C_s	324		**-555.582**					3.68
68B	C_1	294	15.980	-551.451	**-314.375**	-281.011	-265.754	3.68	7.29
68C	C_s	293	12.938	-549.986	-314.147	-281.905	-267.101	7.29	7.78
68D	C_1	283	0.666		-311.913	-286.250	-282.430	7.78	9.67
68E	C_{2v}	283	0.597		-311.516	**-286.263**	-282.554	9.67	11.24
68F	C_s	283	0.573		-311.247	-286.237	-282.588	11.24	11.51
68G	C_{2v}	283	0.552		-310.974	-286.208	-282.618	11.51	13.47
68H	C_{3v}	282	0.031		-311.260	-285.949	**-282.682**	13.47	
69A	C_1	329		**-566.364**	-307.246				3.65
69B	C_1	308		-560.639	-318.206			3.65	4.22
69C	C_{5v}	298	14.909	-559.783	-319.688	-286.265		4.22	5.22
69D	C_s	299	16.223		**-319.820**	-285.837		5.22	7.64
69E	C_s	288	0.705		-317.396	-291.284	-287.367	7.64	9.66
69F	C_1	288	0.653		-317.293	**-291.294**	**-287.462**	9.66	18.06
69G	C_1	286	0.033		-315.850	-290.023	-286.694	18.06	
70A	C_{2v}	335		**-577.740**					3.22
70B	C_1	332		-577.287	-313.363			3.22	3.67
70C	C_5	314		-571.815	-324.212			3.67	4.16
70D	C_{5v}	304	15.324	-570.747	**-325.888**	-291.872		4.16	7.89
70E	C_s	293	0.676		-323.082	**-296.412**	**-292.439**	7.89	17.69
70F	C_s	291	0.035		-321.460	-295.097	-291.707	17.69	
71A	C_1	330		**-588.397**	-316.491				3.42
71B	C_5	320		-583.203	-330.363			3.42	4.28
71C	C_{5v}	310	17.608	-581.945	**-331.589**	-295.612		4.28	7.29
71D	C_{2v}	299	0.695		-329.356	**-302.405**	**-298.405**	7.29	21.50
71E	C_{2v}	296	0.034	-575.523	-326.901	-300.164	-296.719	21.50	
72A	C_1	335		**-599.690**	-320.666				3.40
72B	C_1	314	17.960	-595.065	-335.877	-299.301	-283.195	3.40	4.77
72C	C_s	313	16.818	-592.641	**-336.122**	-299.750	-283.664	4.77	7.29
72D	C_1	303	0.713		-333.968	**-306.460**	-302.387	7.29	10.53
72E	C_1	303	0.695		-333.804	-306.454	**-302.413**	10.53	21.49
72F	C_s	300	0.037		-331.605	-304.245	-300.732	21.49	
73A	C_3	339		**-610.937**	-324.743				3.50
73B	C_s	319	18.316	-603.874	**-341.266**	-304.027	-287.806	3.50	6.97
73C	C_s	318	16.192	-602.727	-340.979	-305.190	-289.451	6.97	7.03
73D	C_s	308	0.725		-339.405	**-311.518**	-307.374	7.03	10.72
73E	C_s	308	0.695		-339.242	-311.503	**-307.421**	10.72	21.49
73F	C_s	305	0.037	-597.775	-336.825	-309.251	-305.732	21.49	

TABLE 2.2: continued.

	PG	n_{nn}	E_{strain}	$\rho_0 = 3$	$\rho_0 = 6$	$\rho_0 = 10$	$\rho_0 = 14$	ρ_{min}	ρ_{max}
59A	C_{3v}	267		**-459.509**	-260.795				3.77
59B	C_{2v}	272		-459.250	-261.475			3.77	4.26
59C	C_1	250	10.832		-267.858	-241.706	-229.054	4.26	4.86
								7.93	9.09
59D	C_{2v}	250	10.939	-453.110	**-267.945**	-241.627	-228.849	4.86	7.93
59E	T_d	240	0.027		-264.710	**-243.331**	**-240.572**	9.09	
60A	C_s	278		**-470.448**					4.51
60B	C_s	255	11.042		**-273.341**	-246.579	-233.702	4.51	9.34
60C	C_s	245	0.540		-269.408	**-247.786**	-244.566	9.34	11.00
60D	C_{2v}	245	0.536		-269.292	-247.782	-244.572	11.00	13.95
60E	C_s	244	0.027		-269.050	-247.371	**-244.579**	13.95	
61A	T_d	284		**-482.026**	-271.693				4.65
61B	C_{2v}	260	11.174		**-278.727**	-251.502	-238.499	4.65	9.54
61C	C_{3v}	249	0.027		-274.135	**-252.397**	**-249.587**	9.54	
62A	C_s	293		**-491.052**	-272.268				4.00
62B	C_s	264	11.707	-485.426	**-283.183**	-255.038	-241.549	4.00	6.33
62C	C_{2v}	264	11.174		-283.103	-255.559	-242.510	6.33	9.24
62D	C_1	254	0.623		-279.852	-256.900	-253.442	9.24	9.78
62E	C_s	254	0.560		-279.460	**-256.908**	-253.555	9.78	10.47
62F	C_1	254	0.526		-279.358	-256.897	**-253.613**	10.47	14.15
62G	C_1	253	0.027	-476.610	-278.482	-256.437	-253.593	14.15	
63A	C_s	301		**-501.732**					3.83
63B	C_1	269	11.880	-497.182	**-288.561**	-259.921	-246.279	3.83	8.87
63C	C_s	259	0.533	495.357	-285.142	**-262.030**	**-258.621**	8.87	14.16
63D	C_s	258	0.027		-283.826	-261.477	-258.600	14.16	
64A	D_{3d}	307		**-512.832**					3.85
64B	C_s	274	12.066	-503.235	**-293.932**	-264.790	-250.989	3.85	8.22
64C	C_{2v}	265	0.552	-501.818	-291.412	**-268.024**	**-264.587**	8.22	24.31
64D	C_s	262	0.031		-289.324	-265.715	-262.643	24.31	
65A	C_s	310		**-523.446**					3.86
65B	C_1	278	12.494		-298.322	-268.407	-254.407	3.86	4.74
65C	C_2	278	12.574	-515.415	**-298.392**	-268.352	-254.301	4.74	6.32
65D	C_1	278	12.081		-298.318	-268.837	-254.984	6.32	8.12
65E	C_{2v}	269	0.603		-296.318	**-272.099**	-268.514	8.12	10.53
65F	C_1	269	0.565		-296.028	-272.084	-268.578	10.53	11.30
65G	C_1	269	0.552		-295.807	-272.070	**-268.595**	11.30	19.72
65H	C_s	267	0.027		-293.515	-270.557	-267.613	19.72	
66A	C_s	314		**-534.464**					3.82
66B	C_1	284	15.128	-530.517	-303.513	-271.712	-256.391	3.82	4.83
66C	C_1	283	12.758	-528.937	**-303.763**	-273.223	-259.079	4.83	7.83
66D	C_s	274	0.640		-301.866	-277.135	-273.454	7.83	9.74
66E	C_s	274	0.573		-301.465	**-277.145**	-273.574	9.74	11.50
66F	C_s	274	0.552		-301.193	-277.116	**-273.602**	11.50	24.31
66G	C_s	271	0.033		-299.454	-274.861	-271.668	24.31	

TABLE 2.2: continued.

	PG	n_{nn}	E_{strain}	$\rho_0 = 3$	$\rho_0 = 6$	$\rho_0 = 10$	$\rho_0 = 14$	ρ_{min}	ρ_{max}
48A	C_{2v}	213		**-346.663**					4.01
48B	C_s	195	7.464	-340.396	**-209.044**	-189.557	-182.618	4.01	9.81
48C	C_s	188	0.461		-204.632	**-189.791**	**-187.516**	9.81	14.72
48D	C_s	187	0.020		-205.419	-189.535	-187.440	14.72	
49A	C_s	219		**-356.413**					3.91
49B	C_{3v}	201	7.770	-350.540	**-215.254**	**-195.275**	-187.212	3.91	10.32
49C	D_{5h}	193	0.471	-337.433	-210.010	-194.828	**-192.504**	10.32	21.18
49D	C_s	191	0.023		-210.023	-193.595	-191.449	21.18	
50A	C_{5v}	224		**-366.636**					4.04
50B	C_s	205	7.770		**-219.820**	**-199.345**	-191.240	4.04	10.12
50C	C_s	197	0.455		-216.105	-199.188	**-196.612**	10.12	15.27
50D	C_1	196	0.023		-215.519	-198.666	-196.462	15.27	
51A	C_2	232		**-376.673**	-217.628				3.74
51B	C_{2v}	210	9.360	-373.933	**-225.391**	-202.912		3.74	9.46
51C	C_s	202	0.863		-221.114	**-203.757**	-200.829	9.46	10.17
51D	C_s	201	0.022		-220.986	-203.737	**-201.474**	10.17	
52A	C_s	238		**-387.587**					3.71
52B	C_{3v}	216	9.618	-384.521	**-231.615**	-208.673	-199.353	3.71	9.36
52C	D_{2h}	207	0.021		-227.346	**-209.769**	**-207.479**	9.36	
53A	D_{6d}	244		**-398.783**					3.70
53B	C_{2v}	222	9.902	-395.150	**-237.835**	**-214.410**	-203.181	3.70	10.32
53C	C_s	211	0.021		-231.694	-213.809	**-211.486**	10.32	
54A	C_s	248		**-407.966**	-232.987				3.41
54B	C_{5v}	228	10.215	-405.832	**-244.058**	**-220.119**	-208.330	3.41	10.32
54C	C_{2v}	217	0.465		-238.115	-219.427	**-216.637**	10.32	15.17
54D	C_{2v}	216	0.021		-237.038	-218.849	-216.492	15.17	
55A	C_1	252		**-417.919**					3.25
55B	I_h	234	10.543	-416.626	**-250.287**	**-225.814**	-213.524	3.25	11.15
55C	C_{2v}	221	0.465		-242.622	-223.482	**-220.646**	11.15	15.18
55D	C_s	220	0.021		-241.385	-222.889	-220.498	15.18	
56A	C_s	258		**-428.611**					3.60
56B	C_{3v}	237	10.545	-425.709	**-253.923**	**-228.900**	-216.538	3.60	10.18
56C	C_{2v}	226	0.481		-248.168	-228.553	-225.633	10.18	11.38
56D	C_s	226	0.465		-248.051	-228.534	**-225.655**	11.38	15.20
56E	D_{2h}	225	0.021	-410.499	-246.729	-227.929	-225.505	15.20	
57A	D_{3h}	264		**-439.960**					4.13
57B	C_s	241	10.563	-436.125	**-258.042**	-232.878	-220.503	4.13	9.61
57C	C_{2v}	231	0.465	-426.762	-253.482	**-233.586**	**-230.664**	9.61	21.83
57D	C_s	229	0.028		-252.749	-232.227	-229.557	21.83	
58A	C_s	267		**-449.432**	-253.759				4.05
58B	C_{3v}	246	10.585	-442.501	**-263.411**	**-237.898**	-225.469	4.05	10.13
58C	C_s	235	0.481		-258.106	-237.660	-234.652	10.13	11.76
58D	C_s	235	0.476		-258.102	-237.649	-234.661	11.76	11.85
58E	C_1	235	0.465		-257.876	-237.631	**-234.671**	11.85	14.94
58F	C_{3v}	234	0.027		-258.241	-237.298	-234.570	14.94	

TABLE 2.2: continued.

	PG	n_{nn}	E_{strain}	$\rho_0 = 3$	$\rho_0 = 6$	$\rho_0 = 10$	$\rho_0 = 14$	ρ_{min}	ρ_{max}
39A	C_{2v}	169		**-258.945**	-158.266				4.48
39B	C_{5v}	153	5.039		**-163.482**	-149.456		4.48	9.46
39C	C_{4v}	148	0.014		-161.702	**-149.887**	**-148.327**	9.46	
40A	C_s	174		**-268.395**	-163.957				4.51
40B	C_s	157	5.040	-263.925	**-167.993**	-153.524	-148.493	4.51	9.51
40C	D_{4h}	152	0.014	-261.116	-165.996	**-153.925**	**-152.334**	9.51	
41A	C_{2v}	180		**-278.406**					4.60
41B	C_s	161	5.040	-273.700	**-172.527**	-157.593		4.60	8.75
41C	C_{2v}	157	0.435		-171.125	-158.506	-156.512	8.75	9.60
41D	C_s	157	0.368	-269.035	-170.808	**-158.521**	-156.631	9.60	11.06
41E	C_{2v}	157	0.366	-267.688	-170.759	-158.518	**-156.633**	11.06	16.83
41F	C_{3v}	156	0.015		-170.898	-158.063	-156.359	16.83	
42A	C_{3v}	186		**-288.335**	-172.252				4.54
42B	C_s	166	5.275	-282.296	**-177.680**	-162.366	-157.125	4.54	9.77
42C	C_s	161	0.368		-175.184	**-162.566**	-160.638	9.77	11.10
42D	C_s	161	0.367		-175.136	-162.564	**-160.641**	11.10	16.82
42E	C_s	160	0.017		-175.405	-162.134	-160.371	16.82	
43A	C_{2v}	192		**-298.172**	-175.540				4.40
43B	C_s	171		-290.632	**-183.093**			4.40	9.34
43C	C_{2v}	166	0.443		-180.838	-167.586	-165.511	9.34	9.57
43D	C_{2v}	166	0.374	-288.302	-180.515	**-167.603**	**-165.635**	9.57	16.67
43E	C_s	165	0.016	-289.533	-180.590	-167.142	-165.371	16.67	
44A	C_{5v}	198		**-308.277**	-179.032				4.38
44B	C_1	175	5.722	-302.004	**-187.626**	-171.071	-165.690	4.38	9.38
44C	C_s	170	0.443		-185.214	-171.631	-169.519	9.38	9.65
44D	C_s	170	0.374	-300.114	-184.841	**-171.645**	**-169.642**	9.65	16.67
44E	C_1	169	0.016		-184.937	-171.182	-169.378	16.67	
45A	I_h	204		**-318.661**	-182.301				4.24
45B	C_1	180	5.965	-310.750	**-192.955**	-175.389	-169.713	4.24	8.75
45C	C_{2v}	175	0.452		-190.548	**-176.666**	-174.510	8.75	11.79
45D	C_{2v}	175	0.451	-303.604	-190.500	-176.663	**-174.512**	11.79	15.10
45E	C_s	174	0.016		-190.275	-176.222	-174.384	15.10	
46A	C_s	207		**-327.033**					3.96
46B	C_{2v}	186	6.646	-320.119	**-199.178**	**-181.236**	-174.605	3.96	10.46
46C	C_s	179	0.452		-194.924	-180.711	-178.518	10.46	11.79
46D	C_s	179	0.451		-194.877	-180.709	**-178.519**	11.79	15.11
46E	C_s	178	0.016		-194.622	-180.262	-178.391	15.11	
47A	C_3	210	40.212	**-336.666**	-194.242	-170.368			4.03
47B	C_1	190	6.648	-331.591	**-203.704**	-185.302	-178.621	4.03	9.60
47C	C_{2v}	184	0.461	-323.011	-200.257	**-185.746**	**-183.508**	9.60	14.94
47D	C_{3v}	183	0.016		-199.964	-185.302	-183.397	14.94	

TABLE 2.2: continued.

	PG	n_{nn}	E_{strain}	$\rho_0 = 3$	$\rho_0 = 6$	$\rho_0 = 10$	$\rho_0 = 14$	ρ_{min}	ρ_{max}
31A	C_1	126		**-185.984**	-122.440				4.60
31B	C_s	126		-185.299	**-122.858**			4.60	6.35
31C	C_s	115	3.490		-122.342	-112.543	-108.723	6.35	8.95
31D	C_s	112	0.276		-121.535	**-113.057**	-111.711	8.95	10.42
31E	C_{2v}	112	0.246	-181.901	-121.367	-113.048	**-111.761**	10.42	20.90
31F	C_s	111	0.011		-120.805	-112.376	-111.240	20.90	
32A	C_{2v}	132		**-195.468**	-127.644				5.93
32B	C_{2v}	120	3.83		**-127.771**	**-117.284**		5.93	10.27
32C	C_s	116	0.269		-125.954	-117.117	-115.733	10.27	11.33
32D	C_1	116	0.260		-125.950	-117.106	**-115.748**	11.33	20.32
32E	C_s	115	0.011		-125.126	-116.416	-115.246	20.32	
33A	C_s	137		**-204.209**	-131.704				5.35
33B	C_{5v}	137		-203.575	-131.774			5.35	5.74
33C	C_s	124	3.832		**-132.287**	-121.352		5.74	8.46
33D	C_{2v}	121	0.313		-131.556	-122.160	-120.666	8.46	9.71
33E	C_{2v}	121	0.269		-131.379	**-122.167**	**-120.741**	9.71	19.88
33F	C_s	120	0.011		-130.467	-121.455	-120.253	19.88	
34A	D_{5h}	143		**-214.068**	-136.468				5.87
34B	C_{2v}	128	3.832	-209.947	**-136.798**	-125.420		5.87	8.52
34C	C_s	125	0.313		-135.989	-126.212	-124.675	8.52	9.79
34D	C_s	125	0.293		-135.973	**-126.214**	**-124.711**	9.79	19.06
34E	C_{4v}	124	0.013		-135.486	-125.616	-124.282	19.06	
35A	C_s	147		**-221.771**	-140.503				4.05
35B	C_{3v}	147		-221.294	-141.106			4.05	5.62
35C	C_1	133	3.975		**-141.957**	-130.282	-126.120	5.62	8.08
35D	C_{2v}	130	0.304		-141.403	**-131.274**	**-129.700**	8.08	18.65
35E	C_{3v}	129	0.011		-140.132	-130.533	-129.265	18.65	
36A	C_s	152		**-230.508**	-144.827				4.68
36B	C_1	152		-229.689	-145.274			4.68	5.07
36C	C_s	138	4.35		**-147.382**	-134.989		5.07	9.51
36D	C_1	134	0.334		-145.985	**-135.313**	-133.656	9.51	10.50
36E	C_s	134	0.314		-145.748	-135.305	**-133.691**	10.50	18.42
36F	C_s	133	0.013		-145.279	-134.701	-133.296	18.42	
37A	C_s	158		**-240.008**	-149.766				5.25
37B	C_1	142	4.35		**-151.891**	-139.056	-134.765	5.25	7.62
37C	C_{2v}	139	0.357		-151.436	**-140.360**	-138.622	7.62	10.57
37D	C_s	139	0.318		-151.078	-140.343	**-138.690**	10.57	18.29
37E	C_s	138	0.014		-150.885	-139.776	-138.308	18.29	
38A	D_2	164	30.138	**-249.159**	-153.209	-134.320			3.15
38B	C_1	163	27.962	-249.088	-154.165	-135.519	-129.339	3.15	4.70
38C	C_s	163		-248.600	-154.042			4.70	4.76
38D	O_h	144	0.013	-246.415	-157.407	**-145.850**	**-144.321**	4.76	5.40
								6.95	
38E	C_{5v}	147	3.714		**-157.477**	-144.756		5.40	6.95

TABLE 2.2: continued.

	PG	n_{nn}	E_{strain}	$\rho_0 = 3$	$\rho_0 = 6$	$\rho_0 = 10$	$\rho_0 = 14$	ρ_{min}	ρ_{max}
19A	D_{5h}	68	6.001	**-90.6475**	**-68.4923**	**-62.1668**	-56.6767		10.70
19B	C_{2v}	61	0.151	-87.4857	-65.0648	-61.4271	**-60.8124**	10.70	
20A	C_{2v}	72	6.507	**-97.4174**	**-72.5078**	**-65.6791**	-61.3272	2.02	10.24
20B	C_{2v}	65	0.162	-94.2224	-69.2027	-65.4237	**-64.7920**	10.24	
21A	C_{2v}	76	7.133	**-104.337**	-76.4873	-69.0687	-65.1796		5.40
21B	C_1	76	6.922	-104.004	**-76.5291**	-69.2763	-65.7789	5.40	9.84
21C	C_s	69	0.169		-73.5770	**-69.4499**	**-68.7836**	9.84	
22A	C_s	81	8.198	**-112.041**	**-81.1367**	-73.0143	-68.5809		9.58
22B	C_1	73	0.169		-77.8879	**-73.4943**	**-72.7917**	9.58	
23A	D_{3h}	87	10.597	**-120.787**	**-86.7355**	-76.6306	-70.8161		8.35
23B	D_{3h}	84	6.097	-116.279	-84.9406	-78.1439	-74.4424	8.35	9.71
23C	C_s	78	0.433		-83.5049	**-78.3254**	**-77.3025**	9.71	22.45
23D	C_1	76	0.007		-82.2527	-76.8988	-76.1575	22.45	
24A	C_s	91	10.947	**-127.885**	**-90.6854**	-80.2955	-74.6137	2.79	8.55
24B	C_1	82	0.434		-87.8204	**-82.3702**	**-81.3095**	8.55	15.34
24C	C_{2v}	81	0.007		-87.6268	-81.9414	-81.1642	15.34	
25A	C_s	96	12.090	**-136.073**	**-95.1279**	-84.1688		2.62	7.76
25B	C_{3v}	87	0.893		-93.3428	**-86.9897**	**-85.4774**	7.76	15.40
25C	C_s	85	0.010		-92.2415	-86.0154	-85.1768	15.40	
26A	T_d	102	15.393	**-145.322**	**-100.550**	-86.8823			7.89
26B	C_{2v}	91	0.491	-138.941	-97.3632	**-91.3703**	**-90.2108**	7.89	14.20
26C	D_{3h}	90	0.008		-97.6487	-91.0851	-90.1893	14.20	
27A	C_s	106		**-152.514**	-104.489				4.72
27B	C_{2v}	106		-151.735	**-104.745**			4.72	7.71
27C	C_s	97	3.076		-102.750	-94.7362	-91.2366	7.71	8.53
27D	C_s	95	0.491	-146.171	-101.723	**-95.4195**	**-94.2198**	8.53	14.22
27E	C_s	94	0.008		-101.920	-95.1213	-94.1956	14.22	
28A	C_s	111		**-160.773**	-108.855				4.82
28B	C_s	111		-160.385	**-108.998**			4.82	6.70
28C	C_{3v}	102	3.369		-108.186	-99.5240	-95.6921	6.70	8.88
28D	C_s	100	0.983		-107.214	**-100.008**	**-98.3317**	8.88	14.57
28E	C_{2v}	98	0.008		-106.239	-99.1611	-98.2021	14.57	
29A	D_{3h}	117		**-170.116**	**-114.146**				6.90
29B	C_1	106	3.370		-112.656	-103.586	-99.7027	6.90	8.95
29C	C_1	104	0.988		-111.544	**-104.051**	-102.333	8.95	11.07
29D	C_{2v}	103	0.246		-111.509	-103.946	-102.744	11.07	11.17
29E	D_{5h}	103	0.225	-164.721	-111.354	-103.927	**-102.775**	11.17	21.90
29F	C_{3v}	102	0.010		-111.135	-103.299	-102.227	21.90	
30A	C_{2v}	121		**-177.579**	-118.116				4.47
30B	C_{2v}	121	8.279	-176.941	**-118.433**	-103.408		4.47	6.86
30C	C_{2v}	109	1.538		-117.011	**-108.571**	-106.426	6.86	12.61
30D	C_s	107	0.238		-115.941	-107.985	**-106.765**	12.61	21.33
30E	C_s	106	0.012		-115.625	-107.368	-106.239	21.33	

TABLE 2.2: Candidate global minima for $N \leq 80$. Energies are given in bold if the structure is the global minimum at that value of ρ_0. ρ_{min} and ρ_{max} give the range of ρ_0 for which the structure is the global minimum. E_{strain} has been calculated at ρ_0=10. If a structure is not stable at ρ_0=10 no value of E_{strain} is given. All energies are given in ϵ.

	PG	n_{nn}	E_{strain}	$\rho_0 = 3$	$\rho_0 = 6$	$\rho_0 = 10$	$\rho_0 = 14$	ρ_{min}	ρ_{max}
5A	D_{3h}	9	0.000	**-9.2995**	**-9.0449**	**-9.0036**	**-9.0003**		
6A	O_h	12	0.000	**-13.5442**	**-12.4878**	**-12.0949**	**-12.0182**		
7A	D_{5h}	16	0.062	**-17.5530**	**-16.2076**	**-15.9565**	**-15.8831**		
8A	D_{2d}	18	0.006	**-22.0429**	-19.1619	-18.2751	-18.0762		5.28
8B	C_s	19	0.062		**-19.3274**	**-18.9646**	**-18.8837**	5.28	
9A	D_{3h}	21	0.002	**-26.7784**	-22.3308	-21.2135	-21.0380		3.42
9B	C_{2v}	23	0.186	-26.6077	**-23.4172**	**-22.8508**	**-22.6449**	3.42	
10A	D_{4d}	24	0.002	-31.5198	-25.5039	-24.2050	-24.0320		2.28
10B	C_{3v}	27	0.694	**-31.8886**	**-27.4733**	**-26.5839**	**-26.1327**	2.28	
11A	D_{4d}	34	10.374	**-37.9308**	-28.7952	-23.6661			3.40
11B	C_{2v}	32		-37.8917				3.40	3.67
11C	C_{2v}	31	0.792		**-31.5219**	**-30.2652**	-29.5881	3.67	13.57
11D	C_s	30					**-29.5961**	13.57	15.29
11E	C_2	30	0.248	-36.6132	-30.6989	-29.8090	-29.5244	15.29	20.60
11F	C_{2v}	29	0.001	-36.6978	-30.4317	-29.2155	-29.0379	20.60	
12A	C_{2v}	38		-43.9713	-35.1999				2.63
12B	C_{5v}	36	1.704	**-44.0979**	**-36.4003**	**-34.3668**	-33.1159	2.63	12.15
12C	C_s	34					-33.1995	12.15	13.03
12D	D_{2d}	34	0.346	-41.8164	-34.8388	-33.7242	**-33.3323**	13.03	17.08
12E	D_{3h}	33	0.001	-42.1214	-34.5680	-33.2223	-33.0383	17.08	
13A	I_h	42	2.425	**-51.7370**	**-42.4399**	**-39.6630**	**-37.2589**		14.76
13B	D_{5h}	37	0.141	-49.9981	-39.3607	-37.2080	-36.7905	14.76	
14A	C_{2v}	46	4.373	**-56.7547**	-44.8275	-41.7170			3.23
14B	C_{3v}	45	2.425	-56.6605	**-45.6193**	**-42.6752**	-40.2598	3.23	13.06
14C	C_{2v}	41	0.141	-55.9716	-43.6340	-41.2493	**-40.7983**	13.06	
15A	D_{6d}	50	9.527	**-63.1621**	-47.5706	-40.5692	-35.7589		3.72
15B	C_{2v}	49	2.573	-62.5939	**-49.7484**	**-46.5414**	-44.0866	3.72	12.71
15C	C_{2v}	45	0.141	-62.6314	-47.9526	-45.2938	**-44.8064**	12.71	
16A	D_{3h}	54	11.222	**-69.1406**	-50.8342	-42.8876			3.39
16B	C_s	53	2.868	-68.7572	**-53.8458**	**-50.2619**	-47.8320	3.39	11.99
16C	C_{2v}	49	0.142	-68.5757	-52.2653	-49.3382	**-48.8145**	11.99	
17A	D_{3h}	58		**-75.6624**	-53.1560				3.42
17B	C_{3v}	57	3.372	-75.1474	-57.8845	-53.7722	-51.3296	3.42	4.88
17C	C_s	57	3.281	-75.0914	-57.9130	-53.8620	-51.4406	4.88	4.91
17D	C_2	57	3.163	-75.0054	**-57.9414**	**-53.9836**		4.91	11.30
17E	C_{2v}	53	0.142	-74.8689	-56.5736	-53.3823	**-52.8226**	11.30	
18A	C_2	65		**-82.5793**	-59.8814			2.14	3.03
18B	C_{5v}	62	4.500	-82.5489	**-62.6892**	**-57.6571**	-54.0597	3.03	10.35
18C	D_{5h}	57	0.142	-81.4902	-60.9265	-57.4297	**-56.8309**	10.35	

decahedral structures are likely to be fewer and longer than those to the icosahedral structures. This effect will be considered in more depth later in the thesis.

It must be emphasized, though, that none of these methods are guaranteed to find the global minimum. Finding the global minima for a PES with so many degrees of freedom is an NP-hard problem[93]. Morse clusters, however, provide an ideal system to compare different global optimization methods both because the complexity of the PES can be systematically varied by changing a single parameter and because this study provides a comprehensive catalogue of likely global minima.

2.3 Results

All the global minima that we have found are catalogued in Table 2.2 along with their energies, point groups, number of nearest neighbours, strain energies and the range of ρ_0 for which they are the lowest in energy. These minima are illustrated in the figures that appear throughout this chapter.

The results are summarized in Figure 2.5 which provides a zero temperature 'phase diagram', showing how the global minimum depends upon N and ρ_0. The structural behaviour of Morse clusters with less than eight atoms is rather uninteresting because the global minimum is independent of ρ_0. For all $N \geq 8$, however, the global minimum changes at least once as a function of ρ_0. For $N \geq 13$, icosahedral, decahedral and fcc structures all exist, and the form of the phase diagram is in very good agreement with the predictions made in §2.2.1. For most sizes the structure changes from icosahedral to decahedral to close-packed as the range of the potential is decreased. For $N < 23$, however, the transition from decahedral to close-packed occurs at larger values than we consider in this study. There are also a number of sizes (N=38–40, 52, 53, 59 and 61) at which there is a transition directly from an icosahedral to a close-packed structure; this occurs when n_{nn} for the lowest energy close-packed structure is greater than or equal to that for the lowest energy decahedral structure. It can be confirmed by examining Table 2.2 that the causes of these transitions are the relative values of n_{nn} and E_{strain}, as we suggested in §2.2.1.

The boundaries between the different morphologies are sensitive functions of N. Such size-dependence is observed for many properties of clusters, and gradually lessens as the size increases (because the addition of a single atom becomes a smaller perturbation) until the bulk limit is reached where properties are continuous functions of N. The decahedral to close-packed boundary is particularly

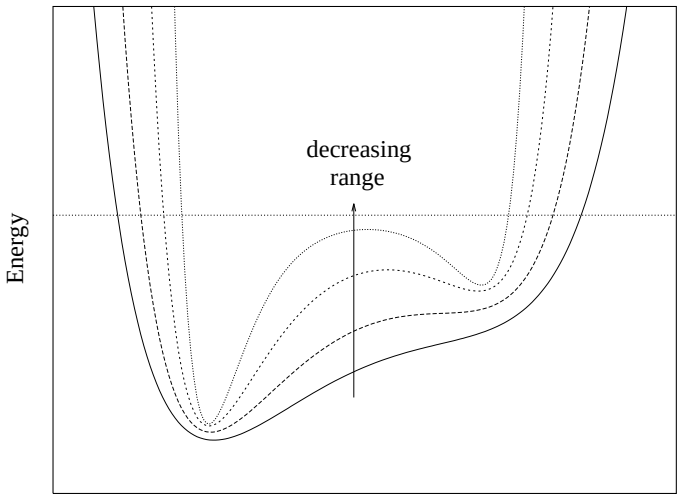

FIGURE 2.4: Schematic diagram to show how a higher energy minimum can be 'swallowed up' by a lower energy minimum as the range of the potential increases.

states on the PES increases with ρ_0. The physical reason for the larger number of minima at short range is the loss of accessible configuration space as the potential wells become narrower, thus producing barriers where there are none at long range. This effect is shown schematically in Figure 2.4.

Barrier heights are also likely to become higher and rearrangements more localized for a shorter-ranged potential. These trends have been observed in comparisons of the rearrangements of 55-particle C_{60} and LJ clusters[90]. Other effects are noted in a detailed analysis of the topography of the M_{13} PES in §6.3. These changes imply that the range of the potential is likely to have a significant effect on the dynamics, making escape from local minima much more difficult. This has been illustrated by Rose and Berry who have shown that the rate at which the ground state structure of a potassium chloride cluster is found upon cooling can be significantly decreased by using a shielded Coulomb potential to reduce the range of the interactions[91]. Similarly, Stillinger and Stillinger[92] and Byth-eway and Kepert[60] both found that minimizations performed from random starting configurations are much more likely to find the global minimum for a long-ranged potential.

Finding the global minimum at short range can also be harder for a more subtle reason. Fcc and decahedral minima have a smaller degree of structural similarity with the large number of minima typical of the liquid-like state than the icosahedral structures. Therefore, the paths from the liquid-like state to the

TABLE 2.1: Number of known stationary points on the PES of M_{13} as a function of ρ_0. The number of stationary points that have not been found as a fraction of the total number is likely to be larger for transition states than minima, and to increase with ρ_0.

	$\rho_0 = 3$	$\rho_0 = 4$	$\rho_0 = 6$	$\rho_0 = 10$	$\rho_0 = 14$
minima	9	159	1441	9290	12717
transition states	27	687	8380	37499	54444

successfully used by Northby to generate low energy icosahedral structures for LJ clusters[50]. The effectiveness of this method is reflected by how few of Northby's lowest energy structures have been superseded and by the length of time that it has taken to find these exceptions[69–73]. As we will show in §2.4, some of the global minima that we have found by this method may be extremely difficult to find by an '*ab initio*' global optimization method. This method, though, does depend on the imagination of the practitioner to conceive of all the possible ways that a structure with a large value of n_{nn} could be obtained. Furthermore, the method will always fail to find the global minima if the latter is not based on one of the ordered types of cluster structure, as is the case for the larger clusters we have considered at low values of ρ_0.

Therefore, complementary to the above method, a number of global optimization techniques were used to try to find structures that might have been missed. First, we used molecular dynamics to explore the PES and generate configurations for minimization. Using high energy runs large regions of the PES are sampled, whereas low energy runs allow a more detailed search of a local region of the PES. Secondly, we used a method in which eigenvector-following is employed to take steps directly between minima on the PES[89]. If low temperature Metropolis Monte Carlo is used in this space of minima, the system will walk down to the bottom of a basin containing many minima. This technique avoids the difficulties associated with trapping in local minima that can occur for methods which take steps directly in configuration space. It is outlined further in Chapter 6. Thirdly, we used a global optimization method developed by David Wales which employs a 'basin hopping' technique.

The above three global optimization methods are least successful for short-ranged potentials. This is because the PES become more rugged as the range is decreased. As illustrated in Table 2.1 for M_{13}, the number of minima and transition

bridge these gaps the tetrahedra have to be distorted, thus introducing strain into the structure. The distance between adjacent vertices of the icosahedron is 5% longer than the distance between a vertex and the centre. Similarly, a pentagonal bipyramid can be considered to be made up of five fcc tetrahedra sharing a common edge. Again, a gap remains if regular tetrahedra are used (Figure 2.3a) and consequently decahedral structures are necessarily strained, although to a lesser extent than icosahedral structures. By contrast, close-packed structures can be unstrained.

Having deduced the relative values of n_{nn} and E_{strain} for icosahedral, decahedral and fcc structures, we can predict the effect of the range on the competition between the three morphologies. For a moderately long-ranged potential, the strain associated with the icosahedral structures can be accommodated without too large an energetic penalty and so they are the most stable. As the range of the potential is decreased, the strain energy associated with the icosahedral structures increases rapidly, and there comes a point where decahedral structures become more stable. Similarly, for a sufficiently short-ranged potential fcc structures become more stable than decahedral structures.

The decomposition of the potential energy also helps us to understand the effect of size on the energetic competition between the three morphologies. The differences in n_{nn} between the morphologies, which arise from their different surface structures, are approximately proportional to the surface area ($\propto N^{2/3}$). The strain energies, though, are proportional to the volume ($\propto N$). Therefore, the differences in E_{strain} increase more rapidly with size than the differences in n_{nn}, thus explaining the changes in the most stable morphology from icosahedral to decahedral to fcc with increasing size. The effect of increasing the size is similar to the effect of decreasing the range of the potential: both destabilize strained structures. The most favourable morphology varies with both the size of the cluster and the range of the potential.

2.2.2 Searching the potential energy surface

The main method that we have used to generate candidate structures for the global minima makes use of the physical insight gained from the last section. We have simply attempted to construct those structures that maximize n_{nn} for the three ordered morphologies. The resulting geometries were then minimized by either the conjugate gradient[87] or eigenvector-following[88] methods. A similar approach was

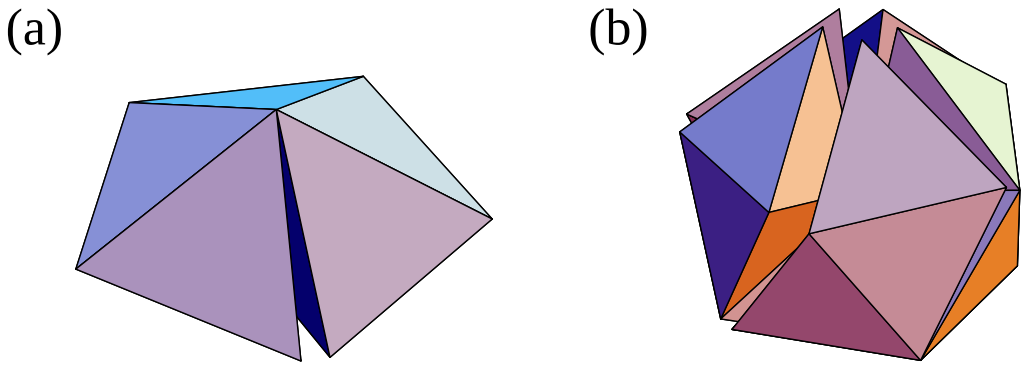

FIGURE 2.3: Examples of the strain involved in packing tetrahedra. (a) Five regular tetrahedra around a common edge. The angle of the gap is 7.36°. (b) Twenty regular tetrahedra about a common vertex. The gaps amount to 1.54 steradians.

differences in n_{nn} arise from surface effects. The optimal shape for each morphology results from the balance between maximizing the proportion of {111} faces (an atom on a {111} face is 9-coordinate, but on a {100} face only 8-coordinate) and minimizing the fraction of atoms in the surface layer. As Mackay icosahedra (Figure 2.1b) have only {111} faces and are approximately spherical, the icosahedral structures have the largest n_{nn}. Complete Mackay icosahedra occur at $N = 13, 55, 147, \ldots$ A pentagonal bipyramid has all {111} faces, but as it is not very spherical more stable decahedral forms are obtained by truncating the structure parallel to the five-fold axis to reveal five {100} faces and then introducing re-entrant {111} faces between adjacent {100} faces. The resulting structure is called a Marks' decahedron (Figure 2.1c) and was first predicted by the use of a modified Wulff construction[85]. The decahedral structures have lower values of n_{nn} than icosahedral structures because of the presence of the {100} faces. The tetrahedron and octahedron are fcc structures that have only {111} faces but they are not very spherical. The optimal fcc structure is the truncated octahedron with regular hexagonal faces (Figure 2.1a). At larger sizes than those considered in this study, the optimal structure involves further facetting, so that it more closely approximates the Wulff polyhedron[86]. Of the three morphologies fcc structures have the lowest values of n_{nn}.

However, icosahedral structures involve the most strain of the three structural types. The Mackay icosahedra can be considered to be made of twenty fcc tetrahedra which share a common vertex. As we see from Figure 2.3b, when twenty regular tetrahedra are packed around a common vertex large gaps remain. To

three contributions as follows,

$$V_M = -n_{nn}\epsilon + E_{\text{strain}} + E_{nnn}. \tag{2.2}$$

The number of nearest-neighbour contacts, n_{nn}, the strain energy, E_{strain}, and the contribution to the energy from non-nearest neighbours, E_{nnn}, are given by

$$\begin{aligned} n_{nn} &= \sum_{i<j, x_{ij}<x_0} 1, \\ E_{\text{strain}} &= \epsilon \sum_{i<j, x_{ij}<x_0} (e^{-\rho_0 x_{ij}} - 1)^2, \\ E_{nnn} &= \epsilon \sum_{i<j, x_{ij}>x_0} e^{-\rho_0 x_{ij}}(e^{-\rho_0 x_{ij}} - 2), \end{aligned} \tag{2.3}$$

where $x_{ij} = r_{ij}/r_0 - 1$, and x_0 is a nearest-neighbour criterion. x_{ij} is the strain in the contact between atoms i and j.

The dominant term in the energy comes from n_{nn}. E_{nnn} is a smaller term and its value varies in a similar manner to n_{nn}. It is only likely to be important in determining the lowest energy structures when other factors are equal. For example, bulk fcc and hexagonal close-packed (hcp) lattices both have twelve nearest neighbours per atom. Next-nearest neighbour interactions are the cause of the lower energy of the hcp crystal when a pair potential such as the LJ form is used[83,84]. Non-nearest neighbour interactions also cause the contraction of nearest neighbour distances from the equilibrium pair value and this contraction increases with the range of the potential[41].

E_{strain}, which measures the energetic penalty for the deviation of a nearest-neighbour distance from the equilibrium pair distance, is a key quantity in this analysis. It should not be confused with strain due to an applied external force. For a given geometry, E_{strain} grows rapidly with increasing ρ_0 because the potential well narrows. This can be seen by taking a Taylor expansion of E_{strain} about $x_{ij} = 0$:

$$E_{\text{strain}} \approx \sum_{i<j, x_{ij}<x_0} \rho_0^2 x_{ij}^2 - \rho_0^3 x_{ij}^3 + 7\rho_0^4 x_{ij}^4/12 + \ldots \tag{2.4}$$

This expansion is valid when $\rho_0 x_{ij}$ is small. To a first approximation the strain energy grows quadratically with ρ_0. Thus decreasing the range destabilizes strained structures.

From this analysis we can see that minimization of the potential energy involves a balance between maximizing n_{nn}, and minimizing E_{strain}. The interior atoms of the three morphologies (Figure 2.1) all have twelve nearest neighbours, and so

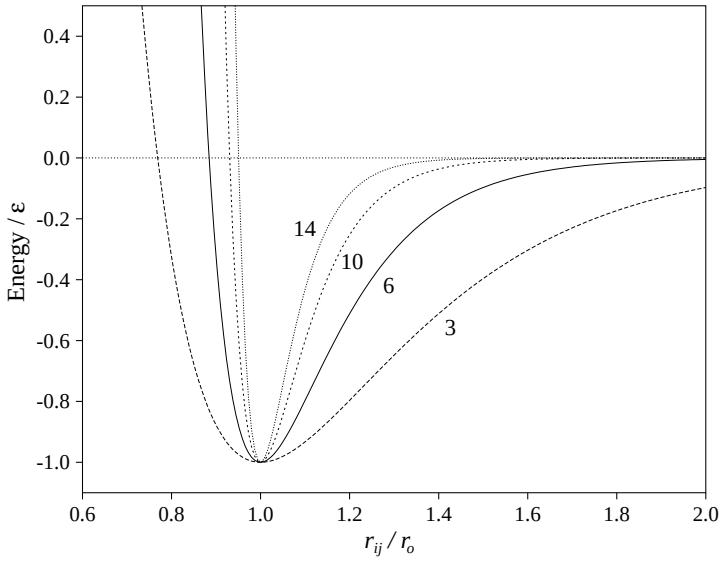

FIGURE 2.2: The Morse potential for different values of the range parameter ρ_0 as marked.

determines the range of the interparticle forces. Figure 2.2 shows that decreasing ρ_0 increases the range of the attractive part of the potential and softens the repulsive wall, thus widening the potential well. Values of ρ_0 appropriate to a wide range of materials have been catalogued elsewhere[78]. Here, we give some representative examples. The LJ potential, which provides a reasonable description of the rare gases, has the same curvature at the bottom of the well as the Morse potential when $\rho_0 = 6$. Girifalco has obtained an intermolecular potential for C_{60} molecules[79] which is isotropic and short-ranged relative to the equilibrium pair separation, with an effective value[80] of $\rho_0 = 13.62$. This potential was designed to describe the room temperature fcc solid phase in which the C_{60} molecules are able to rotate freely. The alkali metals have long-ranged interactions, for example ρ_0=3.15 has been suggested for sodium[81]. Fitting to bulk data gives a value of ρ_0=3.96 of nickel[82].

The structure of a cluster is given by the structure(s) associated with the global free energy minimum. At zero temperature, the structure with the lowest free energy is simply the global minimum of the PES. At higher temperatures, entropic factors must also be considered. Although we only perform a comprehensive survey of the zero Kelvin structure, some examples of the structural effects of temperature are discussed in §2.4.

To understand what factors cause a structure to have low potential energy and how these change with the value of the range parameter, ρ_0, it is instructive to look more closely at the form of the potential. The energy can be partitioned into

hedral, decahedral and close-packed structures. Here we address these issues by examining clusters of atoms bound by the Morse potential. We consider all clusters containing up to 80 atoms, and in particular we attempt to find the global minimum as a function of the range and size.

Such a study provides the most comprehensive model of cluster structure in the literature, having a wider range of applicability and exhibiting a much greater diversity of structural behaviour than observed for LJ clusters, the most well-studied cluster system. The structural catalogue provided by this study will be useful for experimentalists, as they can only obtain indirect structural information which, in order to be assigned, must be compared to that expected for model structures. This is particularly so for chemical probe studies which can obtain detailed information about individual sizes[66–68]. This structural database also provides a useful test of global optimization methods, and would represent a much tougher and more general examination than that provided by LJ clusters which are commonly used as a test system.

The known behaviour of LJ clusters provides a useful starting point for our study. For the majority of small sizes, icosahedral clusters are the lowest in energy. Northby has conducted a systematic survey for $13 \leq N \leq 147$ to find the lowest energy minima based on icosahedral structures[50]. Some of his results have since been superseded[69–73]. Of particular interest are the few sizes at which the lowest energy structures are not icosahedral, but instead decahedral or fcc[70–72]. For larger systems sequences of clusters with the optimal shape for the different morphologies have been compared[74–76]. In these comparisons, the energy is interpolated between the values of N for each cluster of the sequence. The values of N at which the lowest energy lines cross are indicators of the size for which a structural transition is likely to occur. These studies have shown that a decahedral sequence becomes most stable at $N \approx 1600$ and an fcc sequence[76] at $N \approx 10^5$.

2.2 Methods

2.2.1 The potential

The Morse potential[77] may be written as

$$V_M = \epsilon \sum_{i<j} e^{\rho_0(1-r_{ij}/r_0)}(e^{\rho_0(1-r_{ij}/r_0)} - 2), \tag{2.1}$$

where ϵ is the pair well depth and r_0 the equilibrium pair separation. In reduced units ($\epsilon = 1$ and $r_0 = 1$) the potential has a single adjustable parameter, ρ_0, which

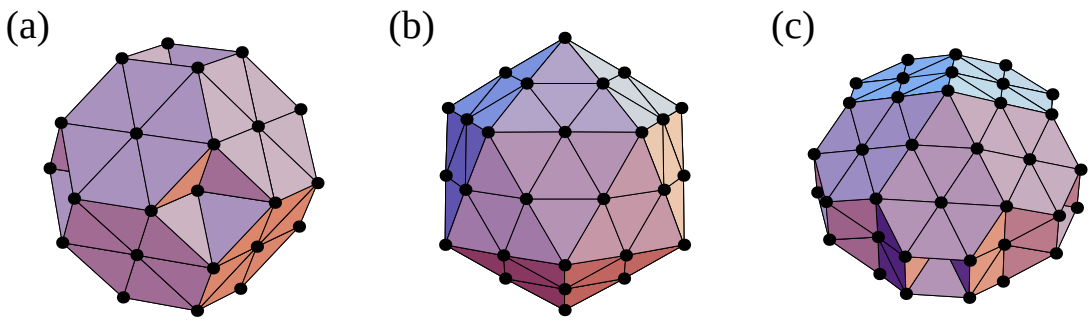

FIGURE 2.1: Three examples of the structures clusters can adopt: (a) a 38-atom truncated octahedron, (b) a 55-atom Mackay icosahedron, and (c) a 75-atom Marks' decahedron. These clusters have the optimal shape for the three main types of ordered packing seen in clusters: face-centred cubic (fcc), icosahedral and decahedral, respectively. The latter two structural types cannot be extended to bulk because of the presence of five-fold axes of symmetry.

cluding metals[51–56], and molecular clusters[57,58]. Icosahedral and decahedral structures are also commonly observed for metal clusters supported on surfaces[1]. At sufficiently large sizes, though, there must be a crossover to the bulk limit where crystalline structures have the lowest energy.

The focus of this chapter is to elucidate the relationship between the form of the interatomic potential and the structure of clusters. Many studies have concentrated on the structures of clusters exhibited by a specific functional form, including model potentials such as the LJ potential and those designed for a particular material. Fewer studies have examined the general structural effects of the different contributions to the potential. For this purpose, it is useful to consider a potential which is simple enough that the effects of any changes made to its form can be understood and that these changes can be made by varying a single parameter. This method has been used to investigate the effect of the range[59–61] and anisotropy[62,63] of the potential on the structure and phase behaviour of small clusters.

In this chapter we further investigate the effects of the range of the potential. Previous studies have found that as the range is increased the number of minima and saddle points on the PES decreases; the PES becomes smoother and simpler[59,64,65]. Furthermore, Bytheway and Kepert noted that, for a sufficiently long-ranged potential, structures based on icosahedral packings become less favoured energetically than structures with even higher coordination[60]. Little, however, has been discovered about the structures associated with shorter-ranged potentials, and the effects of the range and size on the competition among icosa-

Chapter 2
The Structure of Clusters

2.1 Introduction

Structure has a central role in cluster science and is a prerequisite for elucidating many of the properties of clusters. As a consequence, much experimental and theoretical effort has been expended in order to characterize cluster structure. Indeed, many of the experimental methods for obtaining structural information take advantage of the sensitive dependence of cluster properties, such as chemical reactivity[39] and magnetism[40], on cluster structure.

One of the most interesting aspects of cluster structure is the possibility of non-crystallographic symmetry which arises from the absence of translational periodicity. In particular, many clusters are found to have fivefold axes of symmetry. The three main types of ordered structure that simple atomic clusters adopt are close-packed, decahedral and icosahedral. Examples of each are given in Figure 2.1. The decahedral structures have a single fivefold axis of symmetry and are based on pentagonal bipyramids, and the icosahedral structures have six fivefold axes of symmetry.

Icosahedral structures were first discovered in investigations of clusters bound by the Lennard-Jones (LJ) potential[41]. Although early theoretical studies considered structures that were fragments of a crystalline lattice, it soon became clear that the lowest energy structures were based on Mackay icosahedra[42]. The LJ potential provides a reasonable description of the interaction between rare gas atoms, and it has been confirmed by electron diffraction[43–46] and mass spectroscopy[47–49] that rare gas clusters are icosahedral for sizes up to at least 750 atoms. Furthermore, the detailed intensity variations in the mass spectra show very good agreement with those expected from the icosahedral growth sequence of LJ clusters[50]. Icosahedral structures have since been found for many other gas phase clusters, in-